THE JOURNAL OF BIOLOGICAL CHEMISTRY VOL. 289, NO. 13, pp. 8973–8988, March 28, 2014

Structure of Excitatory Synapses and $GABA_A$ Receptor Localization at Inhibitory Synapses Are Regulated by Neuroplastin-65*

Received for publication, August 30, 2013, and in revised form, January 22, 2014 Published, JBC Papers in Press, February 19, 2014, DOI 10.1074/jbc.M113.514992

Rodrigo Herrera-Molina[‡§¶1], Isabella Sarto-Jackson[‖], Carolina Montenegro-Venegas[‡2], Martin Heine[3], Karl-Heinz Smalla[§‡‡], Constanze I. Seidenbecher[‡ ‡‡], Philip W. Beesley[§§], Eckart D. Gundelfinger[‡ ‡‡¶¶], and Dirk Montag[‖‖4]**

From the [‡]Department of Neurochemistry and Molecular Biology, [§]Special Laboratory for Molecular Biology Techniques, [**]Research Group Molecular Physiology, and the [‖‖]Neurogenetics Special Laboratory of the Leibniz Institute for Neurobiology, the [‡‡]Center of Behavioral Brain Sciences (CBBS), and the [¶¶]Faculty of Medicine, Otto von Guericke University, Magdeburg 39118, Germany, the [‖]Department of Biochemistry and Molecular Biology of the Nervous System, Center for Brain Research, Medical University of Vienna, 1090 Vienna, Austria, the [§§]School of Biological Sciences, Royal Holloway University of London, Egham, Surrey TW20 0EX, United Kingdom, and the [¶]Programa de Biología Celular y Molecular, Instituto de Ciencias Biomédicas, Facultad de Medicina, Universidad de Chile, 8380453 Independencia Santiago, Chile

Background: Synaptic excitatory to inhibitory ratio is crucial for brain function but its regulation is poorly understood.
Results: The cell adhesion molecule neuroplastin-65 regulates contact and stability of excitatory synapses and localization of $GABA_AR$ $\alpha2$ subunits at inhibitory synapses.
Conclusion: Neuroplastin-65 mediates specific neuronal connections and regulates the number and function of synapses in hippocampal neurons.
Significance: Correct neuronal network activity in specific brain regions may depend on neuroplastin-65.

Formation, maintenance, and activity of excitatory and inhibitory synapses are essential for neuronal network function. Cell adhesion molecules (CAMs) are crucially involved in these processes. The CAM neuroplastin-65 (Np65) highly expressed during periods of synapse formation and stabilization is present at the pre- and postsynaptic membranes. Np65 can translocate into synapses in response to electrical stimulation and it interacts with subtypes of $GABA_A$ receptors in inhibitory synapses. Here, we report that in the murine hippocampus and in hippocampal primary culture, neurons of the CA1 region and the dentate gyrus (DG) express high Np65 levels, whereas expression in CA3 neurons is lower. In neuroplastin-deficient ($Np^{-/-}$) mice the number of excitatory synapses in CA1 and DG, but not CA3 regions is reduced. Notably this picture is mirrored in mature $Np^{-/-}$ hippocampal cultures or in mature CA1 and DG wild-type ($Np^{+/+}$) neurons treated with a function-blocking recombinant Np65-Fc extracellular fragment. Although the number of GABAergic synapses was unchanged in $Np^{-/-}$ neurons or in mature Np65-Fc-treated $Np^{+/+}$ neurons, the ratio of excitatory to inhibitory synapses was significantly lower in $Np^{-/-}$ cultures. Furthermore, $GABA_A$ receptor composition was altered at inhibitory synapses in $Np^{-/-}$ neurons as the $\alpha1$ to $\alpha2$ $GABA_A$ receptor subunit ratio was increased. Changes of excitatory and inhibitory synaptic function in $Np^{-/-}$ neurons were confirmed evaluating the presynaptic release function and using patch clamp recording. These data demonstrate that Np65 is an important regulator of the number and function of synapses in the hippocampus.

The correct connectivity and function of neuronal networks in the brain is a delicate process that requires the carefully controlled formation, maturation, maintenance, and plastic modulation of synaptic contacts between neurons. Neuronal cell adhesion molecules (CAMs)[5] are crucially involved in these processes (1) as evidenced, for example, in studies of synaptic function and long-term plasticity in hippocampal slices (2–7). More recent findings document CAMs as mediators of specificity in synapse formation and stabilization between neuronal subtypes *in vivo* and *in vitro* (8–10), which is of great importance for the proper function of networks. Here, we report on neuroplastin-65 as a new candidate to participate in these processes.

Neuroplastin-55 (Np55) and -65 are members of the immunoglobulin (Ig) superfamily of single-pass transmembrane CAMs that arise from a single gene by alternative splicing. Np65 possesses three Ig domains, whereas Np55 lacks the N-terminal Ig1 domain

* This work was supported in part by Deutsche Forschungsgemeinschaft Grants SFB426, SFB779, GRK1167, GU 230/6-1, and SM38/8-1), the COST action ECMNet, the Federal State of Saxony-Anhalt, the "European Regional Development Fund" (ERDF 2007–2013), and the Center for Dynamic Systems at the Otto von Guericke University Magdeburg (to D. M., C. I. S., K-H. S., and E. D. G.).
[1] Supported by Deutscher Akademischer Austauschdienst.
[2] Supported by ERANET-Neuron/BMBF AMRePACELL.
[3] Supported by Land Sachsen-Anhalt Research Group Molecular Physiology.
[4] To whom correspondence should be addressed: Leibniz Institute for Neurobiology, Brenneckestrasse 6, 39118 Magdeburg, Germany. Tel.: 49-391-6263-94241; Fax: 49-391-6263-94249; E-mail: montag@LIN-magdeburg.de.

[5] The abbreviations used are: CAM, cell adhesion molecule; VIAAT, vesicular amino acid transporter; MAP, microtubule-associated protein; Np55-Fc, fusion protein comprising Np Ig domains 2–3 fused to human Ig Fc fragment; Np65-Fc, Ig domains 1–3 fused to the Fc fragment; ANOVA, analysis of variance; DG, dentate gyrus; mEPSC, miniature excitatory postsynaptic current; mIPSC, miniature inhibitory postsynaptic current; DIV, days *in vitro*; E/I, excitatory to inhibitory.

(15, 16). Np65, but not Np55, is involved in the adhesion of pre- and postsynaptic elements as: 1) it is localized both presynaptically and postsynaptically (17, 18), 2) it is prominently expressed during the major period of synapse formation in cortex and hippocampus (19), and 3) the Ig1 domain mediates homophilic *trans*-interactions, which modulate synaptic activity (20, 21). Furthermore, Np65 interacts with $GABA_A$ receptor ($GABA_AR$) subunits in hippocampal inhibitory synapses (22). Np65 is also involved in the maintenance of hippocampal CA1 synaptic plasticity and its association with the postsynaptic density protein fraction is regulated by synaptic activity (20, 23). Therefore, it is likely that Np65 regulates formation and/or functional reorganization of excitatory and inhibitory synapses under conditions of basal and increased neuronal activity.

The main focus of the present study was to establish clear roles for the neuroplastins in synapse formation and stabilization and in functional synaptic connectivity. Therefore, we analyzed the numbers of synapses in the CA1, CA2/3, and DG regions of the hippocampus in $Np^{-/-}$ mice. To obtain insight into the underlying subcellular processes and mechanisms we utilized knock-out, fusion protein- and antibody-treated primary hippocampal cultures at different developmental stages to study in detail the role of Np65 in: 1) the formation, stability, morphology, and density of synaptic contacts and spines; 2) the distribution of pre- and postsynaptic protein markers for glutamatergic and GABAergic synapses; 3) the distribution and composition of $GABA_A$ receptors; and 4) the function of both excitatory and inhibitory synapses as determined by patch clamp recording of excitatory and inhibitory postsynaptic currents and by a synaptotagmin uptake assay.

Our data show that Np65 plays a key role in maintaining the structural integrity of excitatory, but not inhibitory synapses. We also provide evidence that Np65 mediates alignment of $GABA_AR$ α2 subunits at postsynapses with vesicular amino acid transporter (VIAAT)-positive presynapses to ensure the correct composition of $GABA_ARs$. Our data suggest that Np65 is an important regulator of the number and activity of synapses in the hippocampus.

EXPERIMENTAL PROCEDURES

Antibodies—Primary antibodies used: rabbit anti-$GABA_AR$ α2 subunit (generously supplied by Dr. W. Sieghart); rat anti-homer (Acris, Herford, Germany); guinea pig anti-synapsin 1,2, guinea pig anti-GAP65, mouse anti-gephyrin, rabbit and guinea pig anti-VIAAT, mouse Cy3-conjugated anti-synaptotagmin-1, guinea pig anti-GABA α2 subunit, and rabbit anti-GABA α1 subunit; guinea pig, rabbit, and mouse anti-microtubule-associated protein 2 (MAP2) (Synaptic Systems, Goettingen, Germany); goat anti-Np65 antibody (RandD Systems, Abingdon, UK); mouse anti-Prox1 (clone 4G10) (Millipore, Schwalbach, Germany); rat anti-Ctip2 (clone 25B6) and mouse anti-GFP (Abcam, Cambridge, UK); mouse anti-β-actin (C4, Santa Cruz Biotechnology, Santa Cruz, CA); rabbit anti-Np Ig 1–3 (20); and rabbit anti-bassoon (24). Secondary antibodies were obtained from Jackson ImmunoResearch (West Grove, PA).

Generation of Neuroplastin-deficient Mice—The first exon of the *neuroplastin* gene encoding the translational start codon and the signal sequence was flanked with 2 lox sites by homologous recombination in embryonic stem cells. Chimeric mice were generated by blastocyst injection of the targeted embryonic stem cells (Karolinska Institute, Stockholm, Sweden). Offspring carrying the floxed *neuroplastin* allele were crossed with transgenic mice expressing Cre recombinase under control of the CMV promoter (25). Cre recombinase-mediated excision resulted in mice carrying a *neuroplastin* allele missing the first exon and, thus, lacking the expression of both Np isoforms. These mice, transmitting the deletion in the germline, were backcrossed to establish heterozygote ($Np^{+/-}$) mice without Cre recombinase transgene. Heterozygote ($Np^{+/-}$) mice were crossed to obtain Np-deficient ($Np^{-/-}$) and wild-type ($Np^{+/+}$) littermates. To confirm the lack of Np expression, protein extracts from brains (Fig. 1*A*) and cultured hippocampal cells were prepared and analyzed by Western blot using standard procedures as described (26).

Cultures of Hippocampal Neurons—Hippocampal neurons were prepared using published protocols (27, 28) with some modifications. To obtain neuronal cultures from genetically modified mice, hippocampi of P0 pups were trypsinized at 37 °C for 8 min and then gently dissociated in minimal essential medium supplemented with 10% horse serum (Invitrogen). Cells were seeded onto poly-D-lysine-coated coverslips using a 1:3 mixture of astroglial conditioned medium and Neurobasal medium supplemented with B27 (Invitrogen). After 1 h, seeding medium was carefully replaced by fresh mixed glial medium. Cultures of rat hippocampal neurons and glia were prepared following published protocols (28). After 14 days, confluent glial cultures in 75-cm^2 flasks were depleted of microglial cells by shaking for 15 min and washing with excess Ca^{2+}/Mg^{2+}-free Hanks' balanced salt solution (Invitrogen). Conditioned medium was obtained by maintaining the monolayer of astrocytes in 10 ml of Neurobasal medium supplemented with B27 for 54–56 h.

Treatment with Neuroplastin Fusion Proteins—Mature neuronal cultures were treated with 0.1 μg/ml of neuroplastin-55-Fc (Np55-Fc, fusion protein comprising Np Ig domains 2–3 fused to human Ig Fc fragment) or neuroplastin-65-Fc (Np65-Fc, Ig domains 1–3 fused to the Fc fragment) or Fc only for 30 min at 37 °C or 15 min at room temperature following published protocols (20, 23). Then cells were carefully washed once with PBS and fixed for fluorescent immunostaining.

Immunostaining of Synaptic Markers and Image Acquisition—Living neurons were incubated with antibodies for 20 min and fixed with 4% *p*-formaldehyde in Hanks' balanced salt solution buffer for 8 min at room temperature. For staining of intracellular proteins, cultures were fixed and then washed with a solution containing 10% bovine fetal serum, 0.1 mM glycine, and 0.1% Triton X-100 in Hanks' balanced salt solution four times for 5 min. To visualize excitatory synaptic contacts, neurons were stained with rat anti-homer (1:500), guinea pig anti-synapsin 1,2 (1:500), or rabbit anti-bassoon (1:500), and mouse anti-MAP2 (1:1000) antibodies for 1 h at room temperature. For inhibitory synapses, staining was done with guinea pig anti-VIAAT (1:1000), mouse anti-gephyrin (1:500), and rabbit anti-MAP2 (1:1000) for 2 h at room temperature. Alternatively, rabbit anti-$GABA_AR$ α2 subunit (5 μg/ml), and guinea pig anti-VIAAT (1:1000) were used for staining. Subsequently, samples

were incubated with anti-mouse Cy5-, anti-rabbit Alexa 488-, anti-rat Alexa 488-, and/or anti-guinea pig Alexa 568-conjugated secondary antibodies (1:1000), all of them generated in donkey. Staining of recombinant proteins adhering to the neuronal cell surface was performed following published protocols (28). For Np65 staining in brain, hippocampal sections were prepared from 2-month-old C57BL6/J mice. Slices were fixed using 4% *p*-formaldehyde followed by 15% ethanol, blocked with 10% horse serum and 0.1% Triton X-100 for 30 min, and incubated with goat anti-Np65-specific antibody overnight. Subsequently, sections were incubated with secondary antibodies, washed, and mounted with Mowiol. Fluorescence was visualized using a Zeiss AXIO Imager A2 microscope equipped with a CCD camera (Visitron Systems) using ×10 (0.45 NA) and ×63 (1.4 NA) objectives. Image acquisition was performed using VisiView software (Visitron Systems, camera binning = 1, pixel size = 0.10238 × 0.10238 μm, pixel depth = 16 bytes). Hippocampal slices of $Np^{+/+}$ and $Np^{-/-}$ mice were prepared, incubated with rat anti-homer (1:500), guinea pig anti-synapsin 1,2 (1:500), or goat anti-bassoon (1:500) antibodies, and mounted as published (28). Slices were photographed using an oil-immersion (HCX APO ×63/1.40 NA) objective coupled to a TCS SP5 confocal microscope under sequential scanning mode and a 6.0-fold digital magnification to reach the Nyquist criteria (80.2 × 80.2 × 209.8 nm voxel dimensions). Z-stacks (41.01 × 41.01 × 5 μm physical lengths) were digitalized in a 512 × 512 pixels format file. Pictures were taken for the CA1 field 50 μm from the midline of the somata and for CA3 75 μm of the *stratum radiatum* (30). For the DG field, we imaged and analyzed areas of the *molecular layer* surrounding the granule cell layer. For Fig. 3*C*, nonlinear correction was applied to original pictures for improved visualization by minimal adjustment in γ settings to 0.9 using Photoshop CS3 version 10.

Identification of Hippocampal Neuronal Type—Neuronal cultures were fixed, permeabilized, and incubated with goat anti-Np65 (1:100), rat anti-homer (1:500), guinea pig anti-MAP2 (1:1000), rat anti-Ctip2 (1:500), and mouse anti-Prox1 (1:500) antibodies for 2 h at room temperature. Subsequently, samples were incubated with anti-rat Alexa 488-, anti-goat Alexa 568-, anti-guinea pig Cy5-, and anti-mouse Alexa 350-conjugated donkey secondary antibodies (1:1000). In some cases, anti-mouse Alexa 488 and anti-rat Cy3-conjugated secondary antibodies (1:1000) were used. In addition, some samples were incubated with 1% DAPI in PBS for 10 min at room temperature.

Image Processing and Puncta Match Quantification—Z-stack images of hippocampal sections were deconvolved using the Huygens Professional software (Scientific Volume Imaging B.V., The Netherlands) and then segmented using the "3D object counter" plugin in the Fiji software (31). Then, from maximal intensity projections, we generated 1-bit mask for each fluorescent channel as described above. For images taken from cultured neurons, each fluorescent image was deconvolved using the adaptive PSF method (10–15 iteration cycles, low-medium noise level) with AutoQuant X2 software (Media Cybernetics, Inc.), and then segmented using Otzu's algorithm. During image processing the original brightness/contrast settings were not modified. For a segmented image of each synaptic marker, 1-bit masks were created using the "analyze particle" in the Fiji software (range of particle size = 0.04–0.5 μm^2 approximately). To quantify the synaptic match, we used binary masks and the "Box_puncta_Ex" and "Match_Set" functions in OpenView software (32). To do this, all puncta in a mask (either postsynaptic to quantify post- to presynaptic match or presynaptic for pre- to post-synaptic match) were detected, and individually boxed in a 1.75 × 1.75 μm matching area centered on their respective center of mass (maximal distance for match detection = 1.25 μm approximately). Each boxed punctum was classified as matched when at least one complementary marker site was detected in the matching area described above. Raw data of distances between matched puncta were automatically generated as an Excel-compatible file for further statistical analysis (for calculations total boxed puncta were considered as 100%). When non-related masks derived from different fluorescent pictures were used, very few false-positive cases of post- to presynaptic "random match" (6.1 ± 0.9%) were detected. Thus, we opted to use this procedure as it was robust in detecting tightly matched complementary synaptic markers. Use of a bigger matching area (2.75 × 2.75 μm, maximal distance for detection = 2 μm approximately) increased the number of apparent matches due to detection both of synaptic markers belonging to the same synapse but also those belonging to neighboring synapses. The random match detection increased up to 40% in many cases and, therefore, the larger matching was not used for analysis. To normalize the number of synaptic puncta, the length of dendrite segments was quantified using the semiautomatic tracing tool in the NeuroJ application of ImageJ.

Quantification of Somatic and Dendritic α2, α1, and Gephyrin Clusters—Living $Np^{+/+}$ and $Np^{-/-}$ cultured hippocampal mouse neurons were stained with guinea pig anti-$GABA_AR$ α2 subunit (1:250), rabbit anti-$GABA_AR$ α1 subunit (1:500) for 20 min, washed, fixed, permeabilized, and incubated with mouse anti-gephyrin (1:500) for 2 h. Subsequently, samples were incubated with anti-rabbit Alexa 488-, anti-mouse Alexa 568-, and anti-guinea pig Cy5-conjugated donkey secondary antibodies (1:1000) for 1 h. Z-stack images of soma and secondary/tertiary dendrites were independently acquired using an oil-immersion (HCX APO ×63/1.40 NA) objective coupled to a TCS SP5 confocal microscope under sequential scanning mode with a 4.0-fold digital magnification, and digitalized in a 512 × 512 pixels format file (61.51 × 61.51 μm physical lengths). We carefully set the lasers power and detection to avoid any fluorescence intensity saturation. All parameter were strictly maintained during the imaging procedure. For these experiments, the size and number of gephyrin puncta were quantified using analyze particle in the Fiji software by setting the next parameters: brightness and contrast range = 30 to 255; color threshold filter pass range = 70 to 255; range of particle size = 0.04–0.6 μm^2. To quantify localization of the α1- and α2-associated fluorescence present in each gephyrin-positive punctum (α1/α2 ratio per gephyrin punctum), we buffered the binary mask of each fluorescent channel in OpenView software (32), and then considered only those clusters of the GABA receptor subunits colocalizing to the corresponding gephyrin clusters as present in the inhibitory postsynapse (box size for matching = 0.425 μm approximately).

Synaptotagmin Uptake Assay—We monitored spontaneous presynaptic activity in hippocampal neurons (21 DIV) pretreated with pre-immune goat IgG or goat anti-Np65 antibody (5 ng/ml) for 15 min at 37 °C. Then cells were briefly washed once with warm Tyrodes buffer (119 mM NaCl, 2.5 mM KCl, 25 mM HEPES, pH 7.4, 30 mM glucose, 2 mM $MgCl_2$, 2 mM $CaCl_2$) and immediately incubated with a mouse Cy3-labeled anti-synaptotagmin-1 antibody (24) in the presence of control goat IgG or goat anti-Np65 antibody for 20 min at 37 °C. Upon uptake, cells were washed twice with Tyrodes buffer, fixed, and stained with rabbit anti-VIAAT (1:1000) and guinea pig anti-synapsin 1,2 (1:500) primary antibodies for 1 h at room temperature. Subsequently, samples were incubated with anti-rabbit Alexa 488-, anti-mouse Cy3-, and anti-guinea pig Cy5-conjugated donkey secondary antibodies (1:1000) for 1 h. Z-stack images of soma and secondary/tertiary dendrites were acquired as described under "Quantification of Somatic and Dendritic α2, α1, and Gephyrin Clusters." We quantified the synaptotagmin-associated fluorescence co-localizing with 1-bit masks derived from VIAAT-positive (inhibitory presynapses) or VIAAT-negative synapsin-positive (excitatory presynapses) puncta using the "image calculator" in the Fiji software. During image processing the original settings of the synaptotagmin channel were not modified. For a segmented image of each presynaptic marker, 1-bit masks were created using the analyze particle in the Fiji software (range of particle size = 0.08–0.5 μm^2 approximately). At least 300 presynapses from 10 neurons per experiment were analyzed.

Electrophysiology—Miniature excitatory postsynaptic current (mEPSC) and miniature inhibitory postsynaptic current (mIPSC) from $Np^{+/+}$ and $Np^{-/-}$ cultured hippocampal mouse neurons (17–24 DIV) were recorded with the patch clamp method in the whole cell configuration. In all cases the experimenter did not know the genotype. Patch electrodes produced from borosilicate glass with a horizontal Brown-Flämming pipette puller (Sutter, Novato, CA) had a pipette resistance of 3–4 megaohm. Intra- and extracellular solutions had the following composition: intracellular 140 mM K-gluconate, 2 mM $MgCl_2$, 4 mM NaATP, 0.1 mM EGTA, 10 mM HEPES, pH was adjusted to 7.25 by 1 M KOH; extracellular 145 mM NaCl, 2.5 mM KCl, 2 mM $MgCl_2$, 2 mM $CaCl_2$, 10 mM HEPES, and 10 mM D-glucose, pH 7.4. To block spontaneous network activity 1 μM tetrodotoxin was added to the extracellular solution. AMPA receptor-mediated mEPSCs were recorded at a holding potential of −70 mV in the presence of 10 μM bicuculline and 10 μM (2*R*)-amino-5-phosphovaleric acid to block $GABA_A$ and NMDA receptors, respectively. $GABA_A$R-mediated mIPSCs were recorded at a holding potential of −40 mV in the presence of 10 μM (2*R*)-amino-5-phosphovaleric acid and 10 μM 6-cyano-7-nitroquinoxaline-2,3-dione. Recordings were performed at room temperature using an EPC 10 patch clamp amplifier (HEKA Electronics, Lambrecht, Germany). Data were acquired and stored using Patchmaster software (HEKA Electronics) and analyzed with Mini-Analysis (Synaptosoft Inc., Decatur, GA).

Statistical Analysis—Raw data distributions were compared using one-way (experimental condition as factor with Kruskal-Wallis H-test) analysis of variance (ANOVA) or two-tailed *t*-test using Origin software. Normalized data classes were evaluated with non-parametric Mann-Whitney U analysis followed by a Kolmogorov-Smirnov test. Statistical significance and corresponding statistical tests are indicated in each figure and in the text.

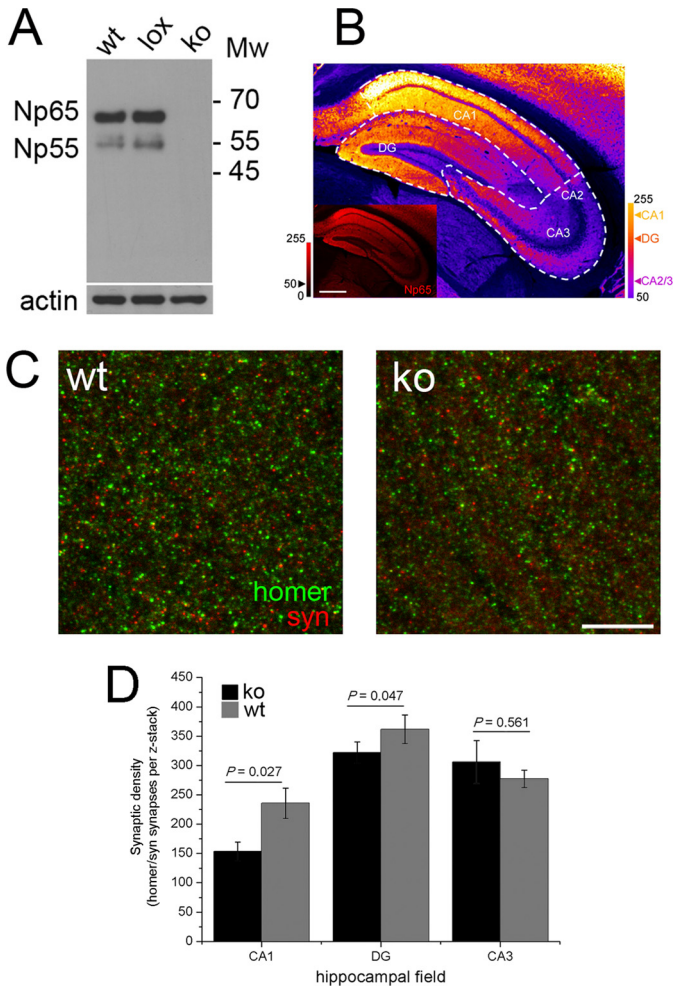

FIGURE 1. **Less excitatory contacts are formed in the hippocampi of Np-deficient mice.** *A,* Western blots of brain homogenates from wild-type (*wt*), floxed *neuroplastin* allele (*lox*), and Np-deficient (*ko*) mice. Actin is a control for sample loading. *B,* quantification of frontal brain sections stained with an isoform-specific anti-Np65 antibody and Alexa 568-coupled secondary antibody. A representative photomicrograph and the corresponding Np65-associated fluorescence intensity scale (*inset left-bottom corner*) are shown. After background subtraction (intensity = 50), Np65-associated fluorescence was quantified for CA1, CA2/3, and DG areas as indicated using ImageJ software (multicolor scale at the *right-bottom corner*). *Scale bar* = 250 μm. *C,* representative maximal intensity projections of entire Z-stacks pictured in the CA1 field from WT (*left*) and KO (*right*) mice are shown. In *green*, postsynaptic compartment staining for homer, and in *red*, presynaptic compartment staining for synapsin (*syn*). *Scale bar* = 10 μm. *D,* quantification of the synaptic density was performed using Z-stack pictures from each indicated hippocampal field in *black bars* for Np-deficient and *gray bars* for wild-type mice. Data are mean ± S.D. from 5 animals per genotype. For each hippocampal field three areas were analyzed in each animal.

RESULTS

Reduction of CA1 and DG Excitatory Synapses in Hippocampal Slices of $Np^{-/-}$ Mice—First, we confirmed that $Np^{-/-}$ mice do not express detectable levels of Np65 or Np55. Whereas Western blots of brain homogenates prepared from wild-type (wt) mice and mice carrying the floxed *neuroplastin* allele (lox) show readily detectable levels of both neuroplastins, homoge-

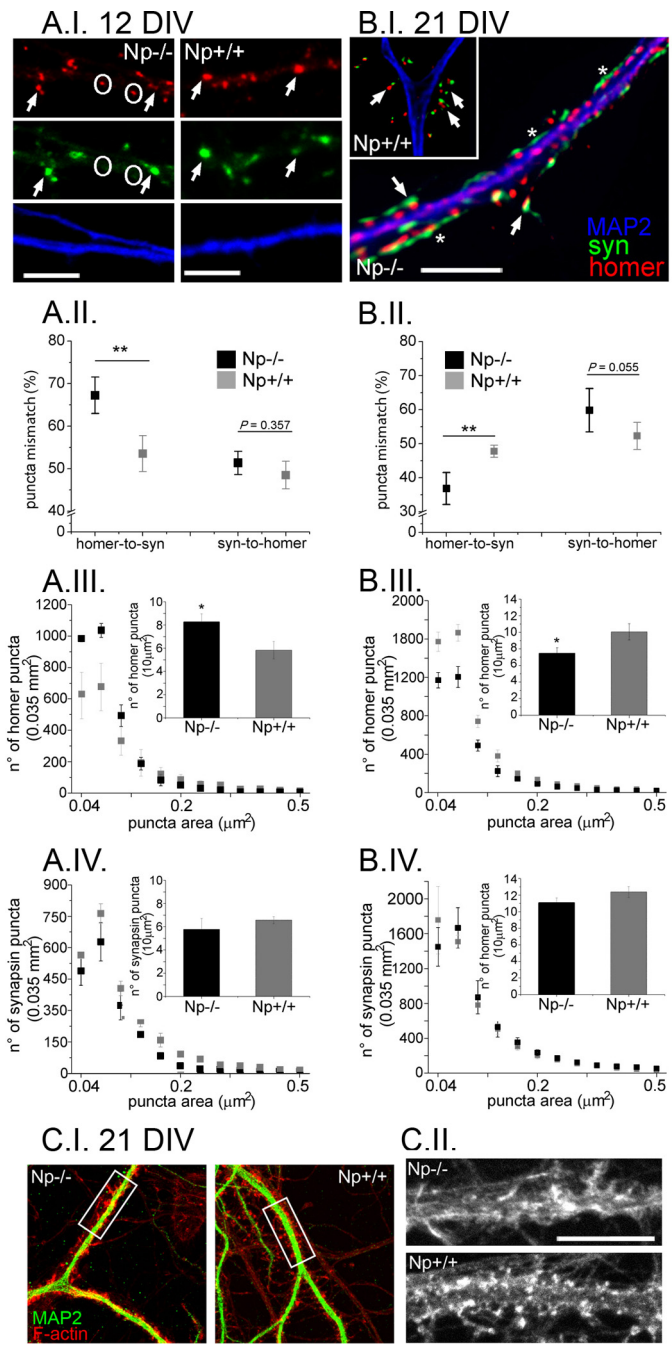

FIGURE 2. **Impaired numbers and matches of excitatory post- and presynaptic sites in $Np^{-/-}$ neurons.** Neurons were stained for homer (*red*), synapsin (*green*), and MAP2 (*blue*) at 12 (*A*, *I–IV*) or 21 (*B*, *I–IV*) DIV and photographed using confocal microscopy. *A*, *I*, maximum intensity projections of fluorescent staining are shown. Note that in $Np^{-/-}$ neurons several encircled homer-positive puncta lack a synapsin-positive presynaptic counterpart. *Arrowheads*, contacts of homer-positive puncta with a presynaptic partner in mutant and wild-type neurons. *B*, *I*, three-dimensional perspectives of Z-stack pictures. *Arrows* indicate well structured synaptic contacts around dendrites. *Asterisks* in $Np^{-/-}$ neurons indicate malformed contacts with diffusely spread presynaptic markers. Quantification of data from neurons lacking Np (*black bars* and *squares*) or wild-type (*gray bars* and *squares*), cultivated for 12 DIV (*A*, *I–IV*) and 21 DIV (*B*, *I–IV*). The percent mismatch of homer to synapsin and synapsin to homer was quantified (*A*, *II* and *B*, *II*). Size distribution of numbers of homer (*A*, *III* and *B*, *III*) or synapsin puncta (*A*, *IV* and *B*, *IV*), and *insets* with the corresponding group summary for each puncta size distribution are shown. Data are mean ± S.D. from 5 independent cultures. **, $p < 0.01$ or *, $p < 0.05$ between genotypes. *C*, $Np^{-/-}$ and $Np^{+/+}$ neurons (21 DIV) were stained with 568-conjugated phalloidin (*red*) and anti-MAP2 antibodies (*green*), and photographed using confocal microscopy. *C*, *I*, maximum intensity projections of fluorescent staining are shown. Indicated digital magnifications of F-actin staining are shown in *C*, *II*. *Scale bar* = 6 μm. Data are mean ± S.D. from 5 independent cultures. *, $p < 0.05$ comparing $Np^{-/-}$ *versus* $Np^{+/+}$ neurons.

nates from Np-deficient (KO) mice show no detectable Np65 or Np55 immunoreactivity (Fig. 1*A*).

Because 1) Np65 expression occurs during formation/stabilization of synapses; 2) Np65 is present in excitatory synapses and its synaptic protein levels are regulated by neuronal activity, and 3) Np65 is expressed much higher in the CA1 and DG subfields than in the CA2/3 area of mouse hippocampus (Fig. 1*B*), we determined whether the absence of Np expression affects the number of excitatory synapses in the hippocampus. Hippocampal slices were stained for homer and synapsin as markers for post- and pre-synaptic compartments, respectively. Then slices were imaged using a confocal microscope and the total number of homer- and synapsin-positive puncta and the synaptic density, *i.e.* total number of synapses per 41 × 41 × 5 μm Z-stack, in the CA1, DG, and CA3 subfields of $Np^{+/+}$ and $Np^{-/-}$ mice was quantified (5 animals per genotype, Fig. 1, *C* and *D*). For $Np^{+/+}$ mice, the number of postsynaptic sites were 480.8 ± 27.1 in CA1, 548.8 ± 42.3 in DG, and 561.2 ± 46.1 in CA3, whereas for $Np^{-/-}$ mice the values were 307 ± 19.5 ($p = 0.021$ *versus* WT CA1, ANOVA), 513.6 ± 59.2 ($p = 0.642$ *versus* WT DG, ANOVA), and 630.4 ± 39.5 ($p = 0.247$ *versus* WT DG, ANOVA). We considered as synapses all puncta of the postsynaptic scaffold protein homer closely matched to a presynaptic marker synapsin-positive puncta ("Experimental Procedures"). We found that Np deficiency reduced the density of synapses in the CA1 and DG, but not in the CA3 subfields (Fig. 1*D*). Thus the densities of synapses in the CA1, DG, and CA3 fields were 235.6 ± 25.9, 361.8 ± 34.3, and 277.4 ± 44.7 in slices from wild-type mice compared with 163.5 ± 15.9 ($p = 0.027$ *versus* WT CA1, ANOVA), 325.2 ± 21.3 ($p = 0.047$ *versus* WT DG, ANOVA), and 306 ± 36.6 ($p = 0.561$ *versus* WT CA3, ANOVA) in the Np-deficient mice (Fig. 1*D*).

Decreased Number of Excitatory Synaptic Contacts in Mature $Np^{-/-}$ Neurons—As a number of CAMs promote neuronal survival, we established that neurons lacking neuroplastin expression survive in culture. No difference in neuronal density (neurons × 10^4 per cm^2) was found comparing cultures derived from hippocampi of wild-type (1.05 ± 0.09, 5 independent cultures) with those from $Np^{-/-}$ mice (1.11 ± 0.07) at 7 DIV. As expected the density of $Np^{+/+}$ and $Np^{-/-}$ neurons decreased as the maturation of cultures progressed to 12 and 21 DIV. However, again no difference in neuronal density between wild-type and $Np^{-/-}$ cultures was observed (0.65 ± 0.04 in $Np^{+/+}$ *versus* 0.71 ± 0.04 in $Np^{-/-}$ at 21 DIV, 5 independent cultures). Moreover, $Np^{+/+}$ and $Np^{-/-}$ neurons displayed nuclei with intact morphology for at least 28 DIV.

To unravel cellular mechanisms responsible for the observed decrease in excitatory synapses in hippocampal slices, we performed triple immunostaining for MAP2, homer, and synapsin in $Np^{-/-}$ and $Np^{+/+}$ neurons cultured for 12 and 21 DIV (29, 33). At 12 DIV, we observed a marked increase in the presence of homer-containing puncta missing a presynaptic counterpart in $Np^{-/-}$ neurons compared with the wild-type (Fig. 2*A*, *I*). At

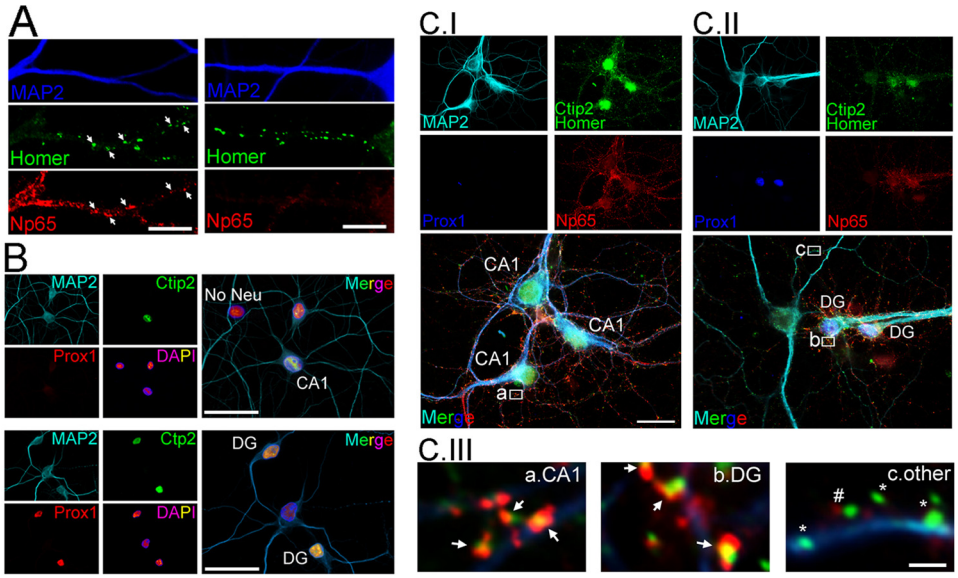

FIGURE 3. **Np65 is highly expressed in CA1 and DG neurons in hippocampal cultures.** Rat hippocampal neurons were stained at 21 DIV for MAP2, homer, and Np65 as well as for Prox1 and Ctip2 to identify neuronal subtypes as indicated below. *A* (*left*), *arrows* indicate a dendritic segment with numerous Np65-positive homer puncta, whereas in *A* (*right*) a dendrite from a different neuron displays lower Np65 expression. *Scale bar* = 5 μm. *B*, identification of CA1 (Ctip2-positive, Prox1-negative) and DG (Ctip2-positive and Prox1-positive) neurons. Nuclei were stained with DAPI. *No Neu* indicates a MAP2-negative non-neuronal cell. In *C*, note that anti-Ctip2 and anti-homer primary antibodies were detected using the same anti-rat Alexa 488-conjugated secondary antibody. Distinguishing the staining for the two antigens was straightforward due to the specificity of the primary antibodies and the characteristic subcellular location of each of these proteins (nuclear *versus* synaptic). *C, I*, shows CA1 neurons expressing very high levels of Np65, whereas in *C, II*, two Np65-positive DG neurons are next to a Prox1- and Ctip2-negative neuron expressing low levels of Np65. In *B* and *C*, *scale bar* = 20 μm. *C, III*, digital magnifications taken from *C, I* and *II* show Np65 (*red*) co-localizing with homer (*green*) in CA1 (*a*) and DG (*b*) neurons (*arrows*). Note that most postsynapses of a Prox1- and Ctip2-negative neuron (*c*) do not display Np65 (*asterisk*) in contrast to a small number of others (# symbol). *Scale bar* = 1 μm. Representative pictures from 4 independent experiments are shown.

21 DIV, $Np^{+/+}$ neurons displayed numerous well formed synaptic contacts around their dendrites, whereas many flattened synaptic contacts were observed in $Np^{-/-}$ neurons (Fig. 2*B, I*). To visualize the F-actin-based cytoskeleton we used 568-conjugated phalloidin and detected numerous malformed dendritic spines in $Np^{-/-}$ neurons (Fig. 2*C*). Together, these results indicate that inactivation of the Np gene may produce a disturbed synaptogenesis due to either reduced formation or reduced stabilization of excitatory synaptic contacts. To evaluate these possibilities we analyzed and compared the presence and the organization of protein markers of excitatory synapses at an early stage of synapse development (12 DIV), and in mature (21 DIV) $Np^{+/+}$ and $Np^{-/-}$ hippocampal cultures by analysis of immunostained cultures. Briefly, images of homer- and synapsin-positive immunofluorescence were deconvolved, segmented to generate independent binary masks, and used to classify each punctum. By this procedure, a synapse is defined as a match of a pre- and postsynaptic punctum due to close proximity, whereas all non-matching puncta are counted as hemisynapses (34, 35) and, therefore, classified as mismatched. The number of synapses was 2.66 ± 0.33 per 10 μm^2 dendrite area for $Np^{+/+}$ and 2.69 ± 0.42 for $Np^{-/-}$ neurons at 12 DIV (120 neurons from 5 independent cultures). Interestingly, at 12 DIV the number of homer-positive postsynaptic sites was 8.1 ± 0.5/10 μm^2 dendrite area for $Np^{-/-}$ neurons, but only 5.8 ± 0.6 for $Np^{+/+}$ neurons ($p < 0.05$ for KO *versus* WT, ANOVA; *inset* in Fig. 2*A, III*). As the number of presynaptic terminals remained unchanged in $Np^{-/-}$ neurons at 12 DIV (Fig. 2*A, IV*), we investigated whether the matching of post- to presynaptic compartments is affected by Np deficiency. Indeed for $Np^{-/-}$ neurons we found a postsynaptic mismatch of 67.2 ± 4.2% compared with a mismatch of 53.5 ± 4.2% in $Np^{+/+}$ neurons ($p < 0.01$ for KO *versus* WT, Mann-Whitney *U* test; Fig. 2*A, II*). Thus, at 12 DIV $Np^{-/-}$ neurons formed a higher number of non-matching homer-containing clusters than $Np^{+/+}$ neurons, whereas the number of excitatory contacts remained unchanged. Surprisingly at 21 DIV, the number of synapses was reduced from 5.21 ± 0.13 for $Np^{+/+}$ to 4.09 ± 0.49 for $Np^{-/-}$ neurons (120 neurons from 5 independent cultures, $p < 0.05$ for KO *versus* WT, ANOVA). Moreover, both the number and percentage of mismatched postsynaptic sites in $Np^{-/-}$ neurons were lower than in the wild-type neurons (Fig. 2*B, II*). The post- to presynaptic mismatch was 36.4 ± 4.7% in mutant compared with 48.6 ± 1.8% in wild-type neurons ($p < 0.01$ for KO *versus* WT, Mann-Whitney *U* test; Fig. 2*B, II*). Thus the mean number of postsynapses per 10 μm^2 of dendrite area was 10.1 ± 0.5 for $Np^{+/+}$ neurons compared with 7.4 ± 0.4 for $Np^{-/-}$ neurons ($p < 0.05$ for KO *versus* WT, ANOVA; *inset* in Fig. 2*B, III*). In contrast, no statistically significant difference for the number of presynapses was found between $Np^{+/+}$ and $Np^{-/-}$ neurons (Fig. 2*B, IV*). These data indicate that the lower number of synapses is accompanied by a decrease of postsynapses and a change in contact with a matching presynaptic site in mature $Np^{-/-}$ neurons.

Differential Expression of Np65 in Hippocampal Neuronal Types—The abundance of Np65 varies between rat hippocampal areas, being highest in the CA1, less in the DG, and lowest in the CA2/3 region (Fig. 1*B*). Thus, we sought to establish whether this differential expression of Np65 is an intrinsic signature that also occurs in dissociated hippocampal neurons in

culture. We found that Np65 expression varies from highly abundant to sparse between individual neurons in culture (Fig. 3*A*). To evaluate whether the differential Np65 expression is associated with a subset of excitatory synapses present on different neuronal subtypes, we used antibodies to stain Np65, homer, and MAP2 in combination with an anti-Ctip2 antibody, which labels CA1 pyramidal neurons and many DG neurons (8, 36), and anti-Prox1 that selectively labels DG neurons (37). Using this combination of antibodies, we were able to distinguish CA1 neurons (Ctip2-positive, Prox1-negative nuclei) and DG neurons (Ctip2-positive and Prox1-positive nuclei) from other neuronal types (Ctip2-negative and Prox1-negative nuclei) (Fig. 3, *B* and *C*). Np65 was abundant in CA1 (Fig. 3*C, I*) and DG neurons (Fig. 3*C, II*) in contrast to the low Np65 levels detected in other neurons (Fig. 3*C, II*). Digital magnifications confirmed that Np65 is tightly associated with CA1 and DG postsynaptic sites (arrows in Fig. 3*C, III, a* and *b*) even though postsynaptic sites in other neuronal types contained no (*asterisk* in Fig. 3*C, IIIc*) or only low levels (*hash sign* in Fig. 3*C, IIIc*) of Np65. Thus, as for the *in vivo* situation, CA1/DG hippocampal neurons express higher levels of Np65 and can localize it to their synaptic contacts *in vitro*.

Np65 Stabilizes Excitatory Synaptic Contacts of CA1 and DG Neurons—Np65 maintains synaptic plasticity of CA1 synapses in rat hippocampal slices as incubation with Np65-Fc fusion protein impairs the maintenance of long term potentiation (20). To enable detailed analysis of synaptic matching, we perturbed Np function by addition of Np-Fc fusion proteins to hippocampal cultures. In particular, we evaluated whether incubation with Np65-Fc or Np55-Fc perturbs the contact of pre- and postsynaptic structures in mature $Np^{+/+}$ neurons. Np55-Fc was not able to modify the contact between homer-positive and bassoon-positive post- and presynaptic compartments because they were similarly abundant and matched as well as under control conditions (Fc protein) (Fig. 4*A*). In contrast, Np65-Fc reduced the amount of synaptic contacts and produced a striking increase of decoupled pre- and postsynaptic sites (Fig. 4*A*). This observation was confirmed by quantifying the post- to presynaptic mismatch as described for Fig. 2 (Fig. 4*B*). The post- to presynaptic mismatch was 61.4 ± 8.5% in Np65-Fc-treated compared with 43.1 ± 7.4% in Fc-treated $Np^{+/+}$ neurons (100 neurons from 4 independent cultures, $p < 0.01$, Mann-Whitney *U* test; *inset* in Fig. 4*B*). In control neurons, 64.7 ± 4.2% of matched puncta were formed by pre- and postsynapses as close as 0.25 μm in proximity, whereas in Np65-Fc-treated neurons only 48.1 ± 5.6% of contacts showed the same proximity (100 neurons from 4 independent cultures, $p < 0.05$, Mann-Whitney *U* test; Fig. 4*B*). Furthermore, Np65-Fc-treated neurons displayed more synaptic contacts in the higher range of pre- to postsynapse distances than control neurons (Fig. 4*B*). To assess the robustness of our quantification and statistics, we calculated the cumulative frequency for matched synaptic contacts as cumulative puncta match (Fig. 4*C*). Np65-Fc-treated neurons presented a lower pre- to postsynaptic match than control neurons throughout the whole range of pre- to postsynapse distances (4 independent experiments, $F_{(1,145)} = 33.345$, $p = 0.023$, one-way ANOVA; Fig. 4*C*). Moreover, particular classes of pre- to postsynaptic distances were significantly

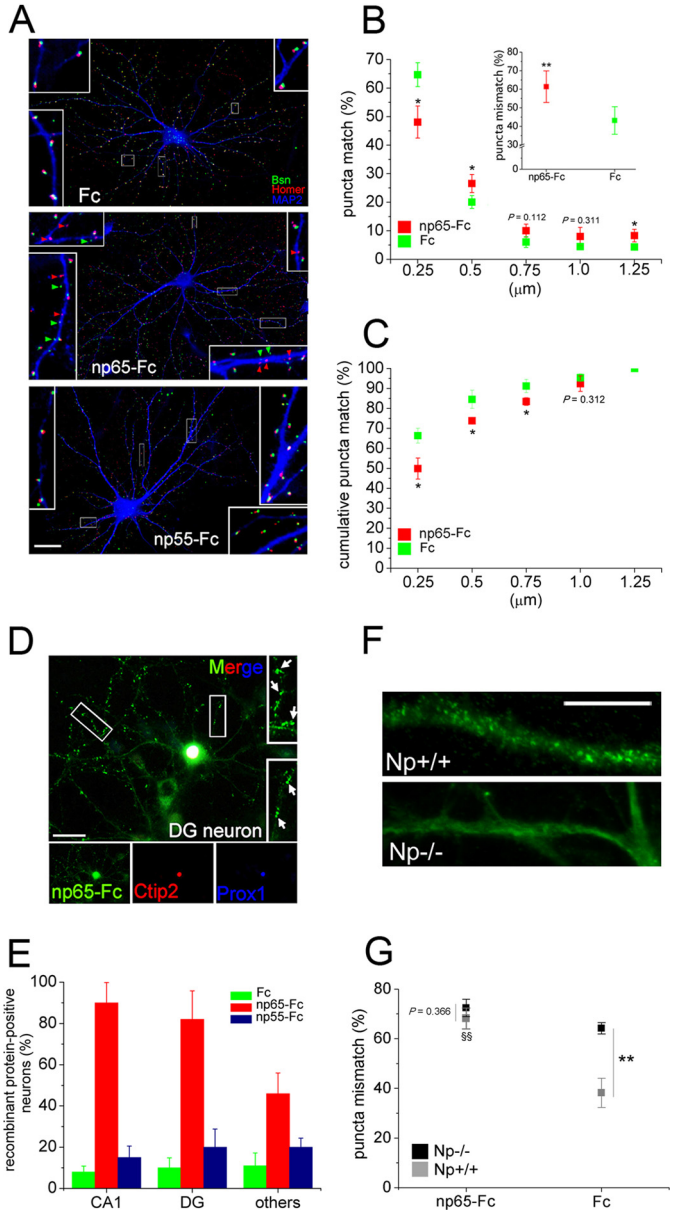

FIGURE 4. **Binding of Np65-Fc to CA1 and DG neurons causes dissociation of excitatory synaptic contacts.** *A–C* and *G*, $Np^{+/+}$ or $Np^{-/-}$ mouse hippocampal neurons (21 DIV) were treated with Fc, Np65-Fc, or Np55-Fc for 30 min at 37 °C, fixed, stained for pre- (Bsn, bassoon, *green*) and postsynaptic (homer, *red*) markers, photographed, and analyzed as described in the legend to Fig. 2. Representative cells are shown, and digital magnifications of different regions from each experimental condition are included. *B*, the *inset* shows the percent of mismatched puncta for Np65-Fc- and Fc-treated cultures. *C*, cumulative frequencies of matched puncta *versus* distance between synaptic markers were plotted taking the value of the number of matched puncta as 100%. *D*, after treatment with recombinant proteins, rat hippocampal neurons were fixed, permeabilized, and classified by immunostaining as described in the legend to Fig. 3. *White arrows* indicate clusters of fusion proteins detected using an Fc fragment-specific FITC-conjugated anti-human IgG antibody (*green*). *E*, quantification of the number of neurons positive for aggregates of recombinant protein was performed following published protocols (28). *F*, magnification of wild-type or mutant neurons after treatment with Np65-Fc detected using an Fc fragment-specific FITC-conjugated anti-human IgG antibody. In *A* and *D*, *scale bar* = 20 μm. In *F*, *scale bar* = 6 μm. *B* and *C*, data are mean ± S.D. from 4 independent cultures, *, $p < 0.05$ comparing Np65-Fc-treated *versus* Fc-treated control neurons. *G*, data are mean ± S.D. from 3 independent cultures, **, $p < 0.01$ comparing Fc-treated $Np^{-/-}$ and $Np^{+/+}$ neurons, §§, $p < 0.01$ comparing Np65-Fc-treated with Fc-treated $Np^{-/-}$ neurons.

decreased in $Np^{-/-}$ compared with $Np^{+/+}$ neurons as indicated in Fig. 4*C* (4 independent experiments, Mann-Whitney *U* test). Thus, when Np65-Fc, but not Np55-Fc, was added to $Np^{+/+}$ hippocampal neurons, a subset of pre- and postsynaptic sites dissociates yielding the observed pattern. These data strongly suggest a specific and acute involvement of Np65 in the structural stability and/or integrity of a population of excitatory synapses.

To evaluate which hippocampal neurons are affected by Np65-Fc, we identified the neuronal subtype to which Np65-Fc binds. After treatment with Fc, Np55-Fc or Np65-Fc neurons were washed, fixed, and the recombinant protein bound to the neuronal surface was detected with FITC-conjugated anti-human IgG antibody specific for the Fc fragments (*green*, Fig. 4, *D* and *E*). Additionally, the neuronal type was determined according to the presence of Ctip2 and/or Prox1 as described above. Aggregates of Np65-Fc were observed decorating the dendritic arborization of CA1 and DG neurons (Fig. 4*D*). In contrast, non-identified neuronal types bound lower amounts of adherent Np65-Fc. Quantification of classifiable neurons decorated with recombinant proteins revealed that indeed CA1 and DG neurons were preferential targets for Np65-Fc, which formed puncta-like aggregates along the dendritic shaft. In contrast, binding of Np55-Fc was comparable with nonspecific binding of control Fc fragments for all the analyzed neuronal types (Fig. 4*E*).

The existence of further cell membrane-bound element(s) binding Np65-Fc is suggested by the fact that residual attachment of the Np65-Fc construct could be detected at the surface of the dendritic shaft of $Np^{-/-}$ neurons (Fig. 4*F*). Therefore, we tested whether Np65-Fc and/or Np55-Fc can affect synaptic stability in Np-deficient neurons. $Np^{-/-}$ and $Np^{+/+}$ neurons were treated with the recombinant proteins, stained with antibodies against homer, synapsin, and MAP2, and the homer to synapsin mismatch was quantified. As expected, the mismatch was increased by 23% in Np65-Fc-treated compared with Fc-treated $Np^{+/+}$ neurons (75 neurons from 3 independent experiments, $p < 0.01$, Mann-Whitney *U* test; Fig. 4*G*). Importantly, Np65-Fc was not able to further enhance the already increased synaptic mismatch in $Np^{-/-}$ neurons ($p = 0.366$, Mann-Whitney *U* test; Fig. 4*G*) indicating that endogenous Np65 is required by Np65-Fc to destabilize synaptic contacts. In addition, incubation with a function-blocking Np65-specific Ig domain antiserum (AS Ig1, 20) drastically decreased both the number of and match between homer- and synapsin-positive synaptic sites in rat hippocampal neurons at 21 DIV (data not shown). In summary these results add further support to the hypothesis that Np65-Fc destabilizes Np65-positive excitatory synaptic contacts by homophilic *trans*-interaction with the endogenous extracellular Np65 domains (20, 21), thus being in agreement with previous data suggesting that synaptic Np65 contacts synapses (20, 22).

The Number of GABAergic Contacts Is Unaffected but the Ratio of Glutamatergic to GABAergic Contacts Is Reduced in Both Np-deficient and Np65-Fc-treated Neurons—In addition to excitatory synapses, the presence of Np65 in GABAergic synapses was established recently (22). We therefore investigated whether matching of somatic and dendritic GABAergic synapses is also affected in $Np^{-/-}$ neurons. We immunostained cultures of 12 and 21 DIV for inhibitory postsynaptic (gephyrin) and presynaptic (VIAAT) markers and found that $Np^{-/-}$ and $Np^{+/+}$ neurons displayed indistinguishable matching of somatic and dendritic GABAergic sites (120 neurons from 5 independent cultures, Fig. 5, *A–D*). Moreover, the number of gephyrin- or VIAAT-positive puncta was not different between $Np^{-/-}$ and $Np^{+/+}$ neurons either at 12 or 21 DIV (see later Fig.

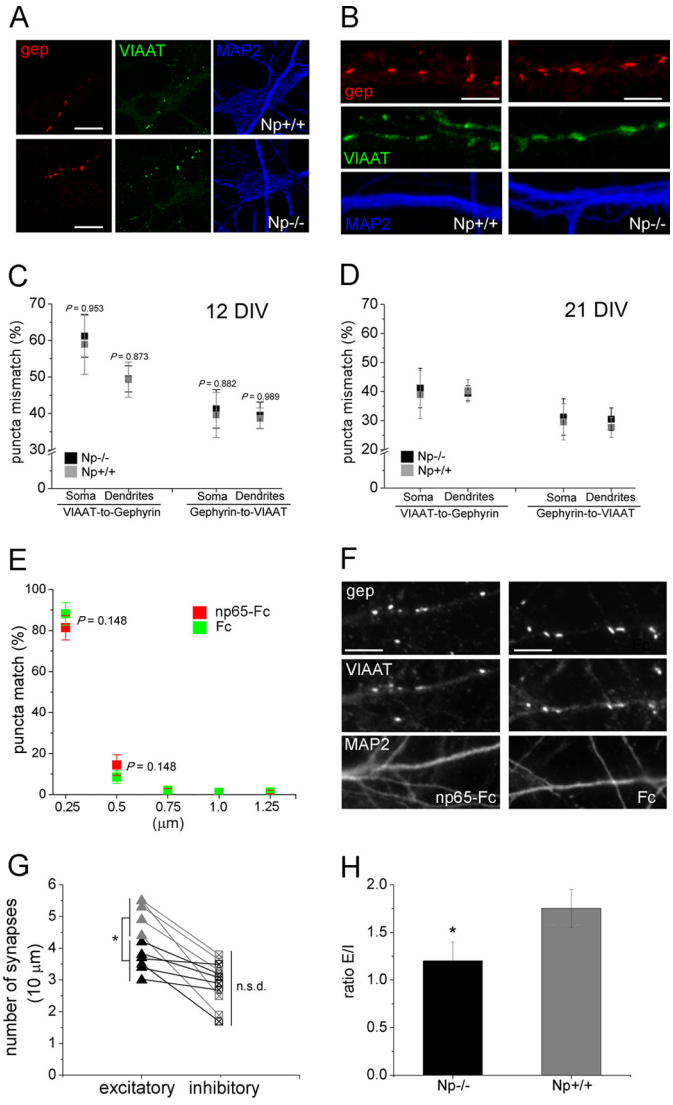

FIGURE 5. **Matching of GABAergic synapses is not modified by Np deficiency or Np65-Fc.** *A–D*, $Np^{+/+}$ and $Np^{-/-}$ hippocampal neurons were cultured for 12 or 21 DIV, stained for gephyrin (*gep*, *red*), VIAAT (*green*), and MAP2 (*blue*), photographed, and puncta mismatch was independently quantified for dendrites and soma as described in the legend to Fig. 2. *E* and *F*, $Np^{+/+}$ neurons were exposed to recombinant Np65-Fc or Fc (control) for 30 min at 37 °C, fixed, and stained. *E*, quantification of the puncta match (fraction of all matched puncta = 100%) *versus* the distance between pre- and postsynaptic sites. Data are mean ± S.D. from at least 5 independent cultures. *G*, quantification of the number of excitatory (total homer to synapsin matched contacts per 10 μm, *green*, $Np^{+/+}$ and *red* $Np^{-/-}$, *triangles*) and inhibitory (total gephyrin to VIAAT matched contacts per 10 μm, in *green*, $Np^{+/+}$ and in *red* $Np^{-/-}$, *squares*) synapses in neurons derived from 6 Np-deficient and 5 wild-type mice. *Lines* connect excitatory and inhibitory contacts from the same culture from a single animal. *H*, the ratio of the number of excitatory to inhibitory synapses (ratio E/I) for each genotype is shown. In *G* and *H*, *, $p < 0.05$; *n.s.d.*, non-significant statistical difference both comparing genotypes. *Scale bars* in $A = 20$ μm, in $B = 5$ μm, and in $F = 6$ μm.

9 and data not shown). This suggests that Np is neither needed to form nor to maintain inhibitory pre- to postsynaptic contacts. To interfere with already established interactions of Np65 in inhibitory synaptic contacts, $Np^{+/+}$ neurons (21 DIV) were treated with Fc protein (control) or Np65-Fc fusion protein for 30 min and stained for gephyrin and VIAAT. Both Fc- and Np65-treated neurons presented well matched inhibitory synapses in dendrites (Fig. 5*F*) and somata (not shown). No statistically significant changes of the pre-postsynaptic site proximity were found after treatment with Np65-Fc. Moreover, the 81.3 ± 5.9% in Np65-Fc-treated and the 88.1 ± 5.5% in Fc-treated neurons of inhibitory contacts were formed by very close apposition (0.25 μm) of pre- and postsynaptic sites (5 independent experiments, $p = 0.148$, Mann-Whitney *U* test Fig. 5*E*). Thus, neither Np deficiency nor acute treatment with Np65-Fc perturb the match of inhibitory synaptic contacts.

If Np65 is necessary for maintenance of the contact of excitatory (Figs. 1–4), but not inhibitory (Fig. 5, *A–F*) synapses, it can be postulated that Np deficiency may affect the ratio of excitatory to inhibitory synapses. To test this hypothesis, cultured hippocampal neurons from individual $Np^{-/-}$ or $Np^{+/+}$ neonate mice were immunostained for excitatory (homer and synapsin) or inhibitory synaptic markers (gephyrin and VIAAT) as well as for MAP2 at 21 DIV. First, we quantified the number of excitatory and inhibitory contacts for each wild-type and mutant culture as for Fig. 2 (Fig. 5*G*). All cultures from individual Np-deficient mice displayed a lower number of excitatory contacts, whereas the number of inhibitory synaptic contacts was essentially the same when compared with $Np^{+/+}$ neurons from individual wild-type mice. We calculated the mean of the ratio of excitatory to inhibitory synapses for each genotype (ratio E/I of cultures derived from 6 deficient and 5 wild-type mice, Fig. 5*H*). Strikingly, this E/I ratio decreased by 30% in $Np^{-/-}$ compared with $Np^{+/+}$ neurons at 21 DIV ($p < 0.05$, Mann-Whitney *U* test, Fig. 5*H*), confirming that Np65 is required for the maintenance of excitatory but not inhibitory contacts.

Acute Treatment with Anti-Np65 Antibodies Differentially Affects Excitatory Versus Inhibitory Presynaptic Function—As Np65 is acutely required for maintaining the structural ratio of excitatory to inhibitory synapses (Fig. 5), it is possible that Np65 is also involved in maintaining the correct excitatory to inhibitory synaptic function. To test this hypothesis we evaluated the spontaneous presynaptic activity, *i.e.* recycling of synaptic vesicles driven by endogenous network activity in the neural cultures. This was reported by the uptake of a Cy3-conjugated antibody against the luminal domain of synaptotagmin (24) in living mature hippocampal neurons where endogenous Np65 was acutely targeted. Therefore we preincubated neurons with an isoform-specific anti-Np65 antibody (see Fig. 8*A*), a manipulation known to block Np65 function (20). After the uptake assays, cells were fixed and stained for presynaptic markers to discriminate between VIAAT-positive inhibitory presynapses and VIAAT-negative synapsin-positive excitatory presynapses. Preparations were photographed using a confocal microscope to distinguish somatic and dendritic compartments (Fig. 6, *A* and *C*). In the somata, the fluorescence intensity of the endocytosed anti-synaptotagmin antibody (uptake intensity, Fig. 6) was 23.4 ± 1.4 arbitrary units per inhibitory presynapse in IgG-treated neurons compared with 26.3 ± 1.6 in anti-Np65-treated neurons (30 neurons from 3 independent experiments, $p = 0.227$, ANOVA, Fig. 6*B*), *i.e.* no significant difference. Importantly the anti-synaptotagmin antibody uptake in excit-

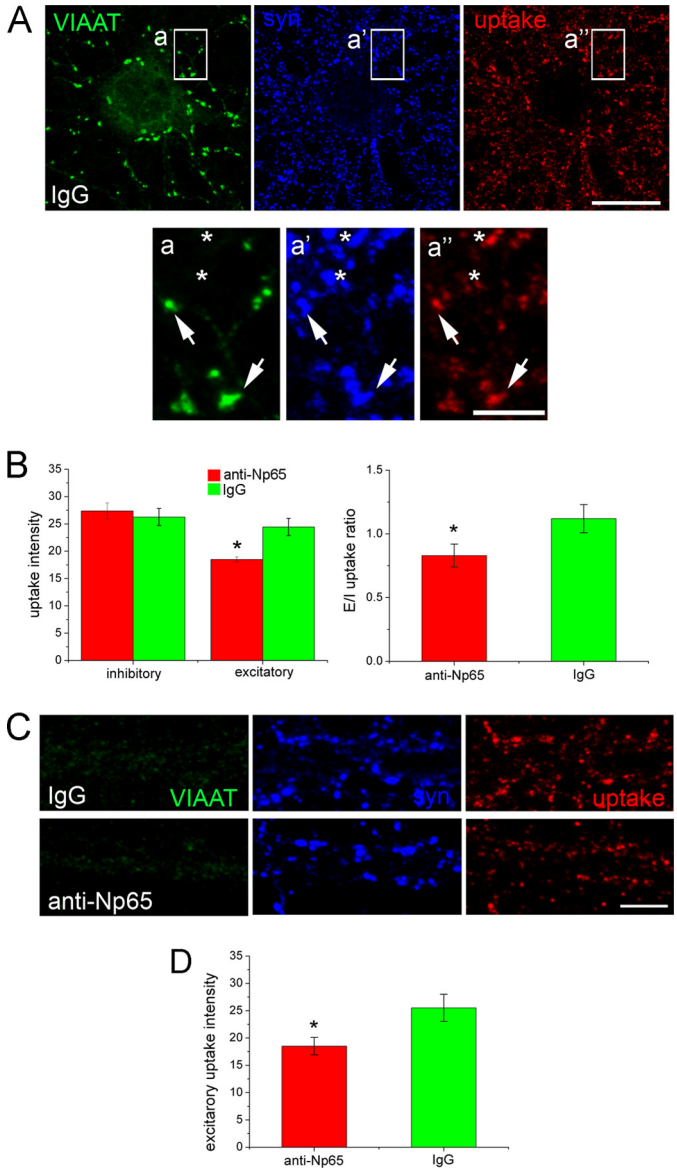

FIGURE 6. **Decreased activity of excitatory presynapses in anti-Np65-treated neurons.** Rat hippocampal neurons were cultured for 21 DIV, treated with normal goat IgG or with goat anti-Np65 antibody for 15 min, incubated with a Cy3-conjugated anti-synaptotagmin antibody (uptake, *red*) for 20 min, washed, fixed, permeabilized, and stained for VIAAT (*green*) and synapsin (*syn*, *blue*). Somatic and dendritic neuronal compartments were independently photographed using a confocal microscope. *A*, an example of the triple fluorescent staining allowing the identification of active inhibitory (*arrows*) and excitatory (*asterisks*) presynapses in the somatic compartment is shown. Digital magnifications of the indicated areas are also displayed in the *lower panel*. *B*, quantification of the intensity of incorporated anti-synaptotagmin antibody (uptake intensity) in inhibitory and excitatory presynapses of IgG- (*green*) and anti-Np65-treated (*red*) neurons. *C*, VIAAT-negative syn-positive excitatory puncta in dendritic segments of IgG- and anti-Np65-treated neurons. *D*, calculation of uptake for excitatory presynapses in dendrites of IgG- and anti-Np65-treated neurons. *Scale bar* in *A*, *upper panel* = 20 μm; in *A*, *lower panel* and *C* = 3 μm. Data are mean ± S.E. from 3 independent experiments. *, $p < 0.05$ between IgG- and anti-Np65-treated neurons.

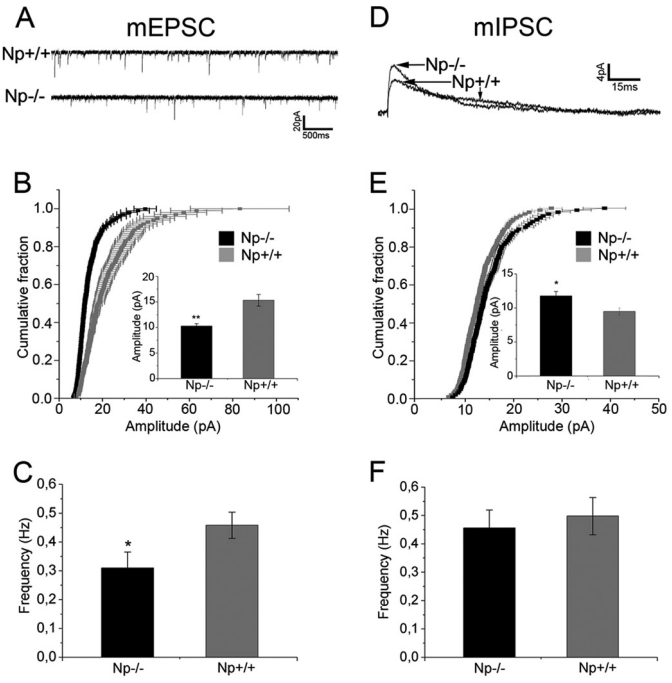

FIGURE 7. **Impaired excitatory and inhibitory synaptic transmission between Np-deficient hippocampal neurons.** $Np^{-/-}$ and $Np^{+/+}$ neurons were impaled under whole cell configuration patch clamp and synaptic activity was recorded. *A*, representative traces of mEPSCs are shown. *B*, quantification of amplitudes of excitatory events *versus* mean cumulative fraction and the mean amplitude (*inset*) in $Np^{-/-}$ (11 cells from 3 independent cultures, 11/3) and $Np^{+/+}$ neurons (13/3). *C*, the mean mEPSC frequency (Hz) was calculated from the data set in *B*. *D*, traces of $GABA_A$-mediated mIPSCs corresponding to an average of 100 events from representative cells are shown. Mean cumulative fraction and mean amplitudes (*E*) as well as frequency of mIPSCs (*F*) were calculated from 10 wild-type and 9 mutant cells from 3 independent cultures. **, $p < 0.01$, or *, $p < 0.05$ between genotypes.

atory presynapses was decreased by acute anti-Np65 antibody treatment. Indeed, the uptake in somatic excitatory presynapses was 24 ± 3.16 in IgG-treated but only 19.5 ± 0.9 in anti-Np65-treated neurons ($p < 0.05$, ANOVA, Fig. 6*B*). The calculated excitatory to inhibitory presynaptic uptake ratio was decreased by 25% from 1.12 ± 0.11 in IgG-treated to 0.83 ± 0.09 in anti-Np65-treated neurons ($p < 0.05$, ANOVA, Fig. 6*B*).

Then we evaluated whether acute treatment with anti-Np65 antibody decreases the synaptic vesicle cycling in excitatory presynapse of dendritic segments where VIAAT-positive inhibitory presynapses are absent (Fig. 6*C*). We observed a conspicuous decrease in the fluorescence intensity of incorporated anti-synaptotagmin antibody in excitatory presynapses of anti-Np65-treated compared with normal IgG-treated neurons (Fig. 6*C*). Quantification revealed that the uptake in excitatory presynapses was 25.5 ± 2.5 in IgG-treated but only 18.5 ± 1.5 in anti-Np65-treated neurons ($p < 0.05$, ANOVA, Fig. 6*D*).

Neuroplastin Deficiency Impairs Excitatory and Inhibitory Synaptic Transmission—As our data indicated impaired formation/stabilization of excitatory contacts in $Np^{-/-}$ neurons, we evaluated electrophysiological alterations at the synaptic level. Spontaneous mEPSC (representative traces in Fig. 7*A*) were recorded using whole-cell patch clamp configuration from $Np^{-/-}$ and $Np^{+/+}$ neurons at 17–24 DIV. Plotting of the cumulative fraction of the peak amplitudes indicated that excitatory synaptic events are significantly smaller in $Np^{-/-}$ than in $Np^{+/+}$ neurons (Fig. 7*B*). The mean amplitude for $Np^{+/+}$ neurons was 15.33 ± 1.15 pA, but only 10.27 ± 0.46 pA for $Np^{-/-}$ neurons (13 $Np^{+/+}$ and 11 $Np^{-/-}$ neurons from 3 independent cultures, $p < 0.01$, Student's *t* test, *inset* in Fig. 7*B*). The frequency of synaptic events was 0.45 ± 0.37 Hz for $Np^{+/+}$ neurons, but only 0.31 ± 0.05 Hz for $Np^{-/-}$ neurons ($p < 0.05$, *t* test, Fig. 7*C*). Kinetic parameters such as the rise time or decay time (τ_{decay}) were undistinguishable between mutant (rise time = 0.51 ± 0.05 ms; τ_{decay} = 3.92 ± 0.33 ms) and wild-type cells (rise time = 0.55 ± 0.04 ms; τ_{decay} = 4.45 ± 0.37 ms). Thus, in good agreement with the anatomical data, spontaneous excitatory synaptic transmission events are reduced in both amplitude and number in $Np^{-/-}$ compared with $Np^{+/+}$ neurons.

We then studied $GABA_A$R-mediated mIPSCs (representative traces in Fig. 7*D*) in $Np^{-/-}$ and $Np^{+/+}$ neurons at 17–24 DIV. Although there was no change in the number and alignment of inhibitory synapses (see above), the amplitude of the mIPSCs was increased by some 24% in $Np^{-/-}$ compared with $Np^{+/+}$ neurons (Fig. 7, *D* and *E*), whereas their frequency was unaffected (Fig. 7*F*). Surprisingly, τ_{decay} was significantly reduced from 29.35 ± 2.28 in $Np^{+/+}$ to 22.64 ± 1.12 in $Np^{-/-}$ neurons (10 $Np^{+/+}$ and 9 $Np^{-/-}$ neurons from 3 independent cultures, $p = 0.0198$, Student's *t* test), whereas the rise time of 0.93 ± 0.29 in $Np^{+/+}$ neurons remained unchanged at 0.85 ± 0.31 in $Np^{-/-}$ neurons ($p = 0.4902$, Student's *t* test). Thus, inhibitory synaptic currents mediated by the $GABA_A$R are perturbed in $Np^{-/-}$ neurons.

Reduction of $GABA_A$ Receptor α2 Subunit in Inhibitory Synapses of Np-deficient Neurons—Because 1) loss of neuroplastin produces perturbed inhibitory synaptic currents (Fig. 7), 2) Np65 is normally expressed in glutamic acid decarboxylase (GAD65)-positive GABAergic axons (Fig. 8*B*), and 3) Np65 co-localizes with the $GABA_A$ receptor α2 subunit at inhibitory synapses in hippocampal neurons (22), we tested whether the localization of α2 subunits is altered in the mutant neurons. We assessed whether $GABA_A$R α2 subunits co-localize with Np65 on the surface of living neurons using an isoform-specific anti-Np65 antibody for native immunostaining (Fig. 8*A*), and we observed a robust co-localization of Np65 with $GABA_A$R α2 subunits on the surface of dendrites (Fig. 8*C*). Immunostaining and confocal microscopy revealed a clearly decreased matching between postsynaptic $GABA_A$R α2 subunits and presynaptic VIAAT on dendrites but not in the somata of $Np^{-/-}$ compared with $Np^{+/+}$ neurons at 7–12 DIV (Fig. 8*D*). On dendrites of $Np^{+/+}$ neurons 23.3 ± 3.4% of the total α2 subunit-associated immunoreactivity was detected co-localizing (below optic resolution distance) with VIAAT. This is in good agreement with previous reports (38). In contrast, $GABA_A$R α2 subunit staining was much more diffuse on dendrites of $Np^{-/-}$ neurons where only 8.9 ± 2.9% was found co-localized with VIAAT (100 neurons from 4 independent experiments, $p < 0.01$, Mann-Withney *U* test, Fig. 8*D*). To assess the synaptic location of α_2 subunits on somata and dendrites, we calculated separately the α_2 to VIAAT match as described above for synaptic markers in these neuronal compartment (box size for matching = 0.875 μm). In dendrites, $Np^{+/+}$ neurons displayed an α_2 to VIAAT match of 72.1 ± 4.9%, whereas this parameter was only 49.2 ±

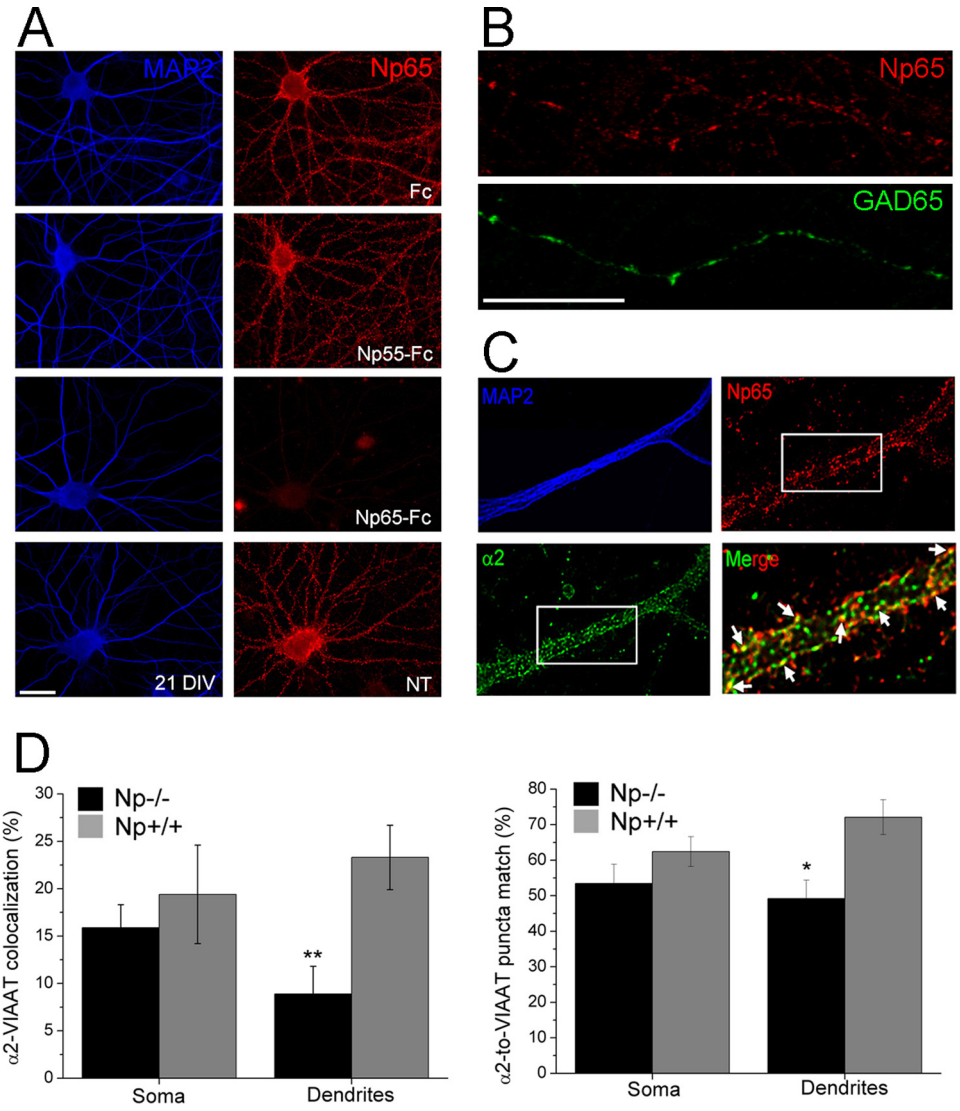

FIGURE 8. **Absence of Np65 leads to altered localization of α2 subunit-containing $GABA_AR$.** *A,* Np65-specific immunodetection in neuronal cultures. To test specificity of Np65 staining, goat anti-Np65 antibody was preincubated with 25-fold excess of different recombinant proteins before application to live hippocampal neurons (21 DIV). When anti-Np65 antibody was preincubated with Np65-Fc, but not with Fc or Np55-Fc, endogenous Np65 was no longer detected on the neuronal cell surface. *NT*, Np65 antibody not pretreated. *B*, rat hippocampal neurons were fixed, permeabilized, and stained for Np65 (*red*) and GAD65 (*green*) at 12 DIV. Axons were recognized as they are thin and long neurites with a constant diameter. *C,* live rat hippocampal neurons were stained for $GABA_AR$ α2-subunits (α2, green), Np65 (*red*), and MAP2 (*blue*) at 7 DIV. Pictures were obtained by confocal microscopy and image deconvolution. Representative pictures of 4 independent experiments are shown. *D*, $Np^{-/-}$ and $Np^{+/+}$ neurons were fixed, stained for $GABA_AR$ α2-subunits (α2, *green*), VIAAT (*red*), and MAP2 (*blue*) at 7–12 DIV, and photographed using a fluorescent microscope. Quantification of co-localization between postsynaptic α_2 $GABA_A$ receptor subunits and presynaptic VIAAT was assessed by fluorescent signal overlap below optic resolution (*C*, *upper graph*). Quantification of the percentage of α_2 *versus* VIAAT puncta match (total number of VIAAT-positive puncta is 100%, match distance = 0.825 μm, *bottom graph*). Data are mean ± S.E. from 4 independent experiments. *Scale bars* = 20 μm. **, $p < 0.01$, or *, $p < 0.05$ between genotypes.

5.2% for $Np^{-/-}$ neurons ($p < 0.05$, Mann-Withney *U* test, Fig. 8*D*). In contrast, the somatic α_2 to VIAAT match was not statistically different between $Np^{-/-}$ and $Np^{+/+}$ neurons (Fig. 8*D*). Thus, Np deficiency produces partial loss of synaptic location of the $GABA_AR$ α2 subunits confirming that Np65 is involved in their positioning at inhibitory synapses.

Increased α1/α2 Ratio in Larger Inhibitory Postsynapses in $Np^{-/-}$ Neurons—To further understand why $GABA_AR$ currents are perturbed in $Np^{-/-}$ neurons, we performed live-cell co-immunostaining of $GABA_AR$ α2 and α1 subunits, before fixation and permeabilization and subsequent staining for gephyrin. To extend the analysis of the $GABA_AR$ composition to somatic and dendritic inhibitory postsynapses in $Np^{+/+}$ and $Np^{-/-}$ neurons at 12 (Fig. 9*A*) and 21 DIV (Fig. 9*B, I* and *II*), we applied confocal microscopy. Although the fluorescence intensity of somatic gephyrin puncta was statistically higher in $Np^{-/-}$ compared with $Np^{+/+}$ neurons at 12 DIV (44.9 ± 1.4 arbitrary units for $Np^{-/-}$ and 38.1 ± 1.2 arbitrary units for $Np^{+/+}$, $p < 0.05$, ANOVA, Fig. 9*C*), no differences were found for this parameter at 21 DIV (Fig. 9*D*). At 12 DIV, in the somatic compartment, $Np^{+/+}$ neurons displayed 180.1 ± 21.1 clusters of gephyrin per somata including 10 μm of the initial segment of primary dendrites although this parameter was 204.5 ± 17.9 for $Np^{-/-}$ neurons (45 neurons, 3 independent cultures, $p = 0.405$, ANOVA, Fig. 9*C*). $Np^{+/+}$ neurons displayed 120.2 ± 35.1 and $Np^{-/-}$ neurons 136.4 ± 17.2 gephyrin-positive clus-

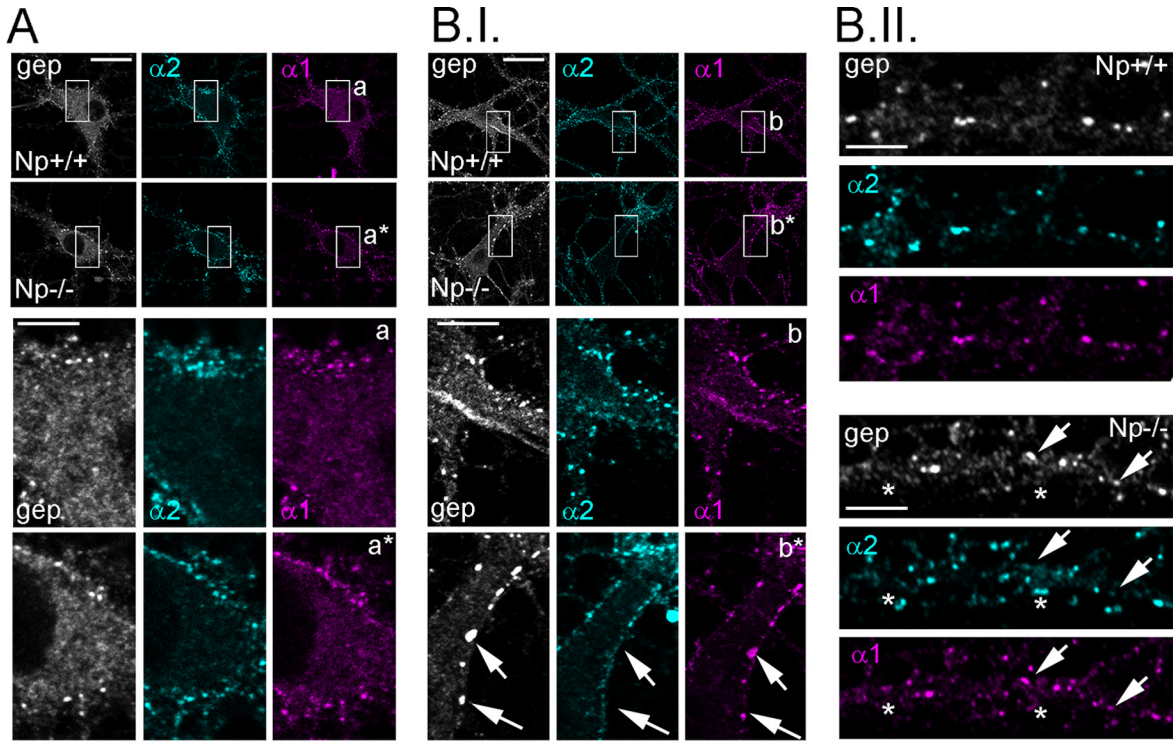
A
B.I.
B.II.
gep
α2
α1
Np+/+
Np-/-
a
a*
b
b*

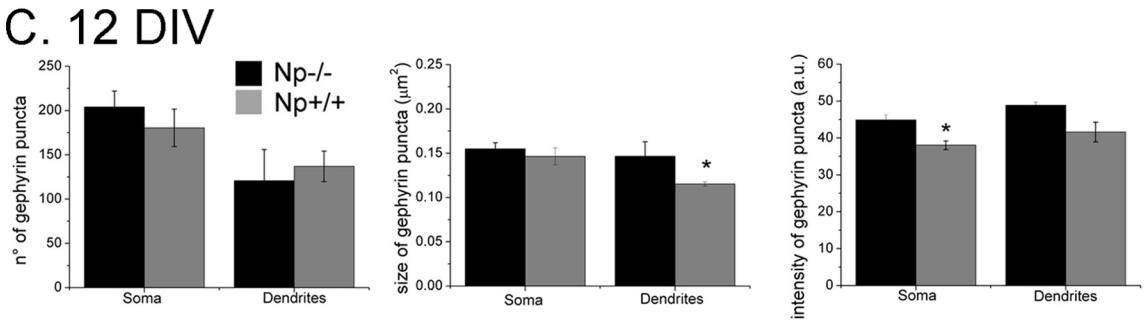
C. 12 DIV
Np-/-
Np+/+
n° of gephyrin puncta
size of gephyrin puncta (μm²)
intensity of gephyrin puncta (a.u.)
Soma
Dendrites

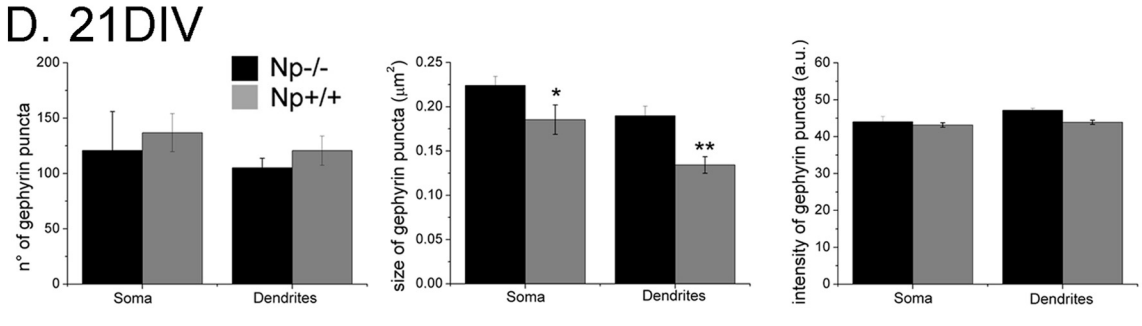
D. 21DIV
Np-/-
Np+/+
n° of gephyrin puncta
size of gephyrin puncta (μm²)
intensity of gephyrin puncta (a.u.)
Soma
Dendrites

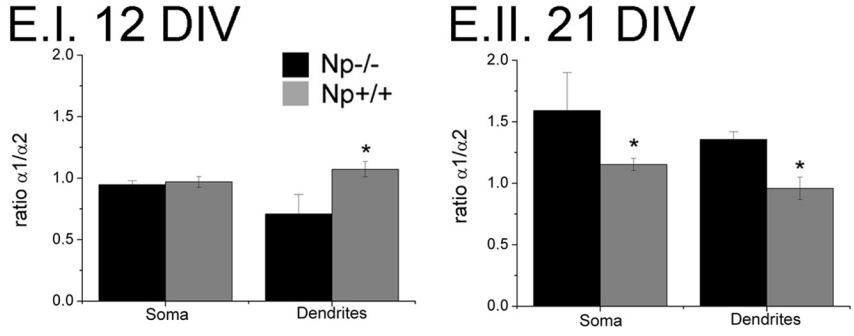
E.I. 12 DIV
E.II. 21 DIV
Np-/-
Np+/+
ratio α1/α2
Soma
Dendrites

ters per 150-μm dendrite ($p = 0.188$, ANOVA, Fig. 9*C*). At 21 DIV, we counted 120.4 ± 33.2 in $Np^{+/+}$ and 131.4 ± 14.2 gephyrin-positive clusters per soma in $Np^{-/-}$ neurons (45 neurons, 3 independent cultures, $p = 0.659$, ANOVA, Fig. 9*D*); whereas that in dendrites, 105.1 ± 8.6 in $Np^{+/+}$ and 119.5 ± 13.2 in $Np^{-/-}$ neurons ($p = 0.328$, ANOVA, Fig. 9*D*). Accordingly, in agreement with the above data (Fig. 5), the number of GABAergic synapses is not changed by Np deficiency at either 12 or 21 DIV. However, the size of the gephyrin-positive puncta was increased in $Np^{-/-}$ compared with $Np^{+/+}$ neurons at 21 DIV. In the somatic compartment of $Np^{-/-}$ neurons the size of gephyrin clusters was 0.224 ± 0.01 and 0.185 ± 0.02 μm^2 in $Np^{+/+}$ neurons ($p < 0.05$, ANOVA, Fig. 9*D*). In dendrites the cluster sizes were 0.190 ± 0.01 μm^2 for $Np^{-/-}$ and 0.134 ± 0.03 μm^2 for $Np^{+/+}$ neurons ($p < 0.01$, ANOVA, Fig. 9*D*).

Then we analyzed the location of the $GABA_AR$ α2 subunits. At 12 DIV, we confirmed that α2, but not α1, is diminished in gephyrin-positive inhibitory postsynapses in dendrites, but not in soma, and at 21 DIV in both somata and dendrites of cultured $Np^{-/-}$ neurons (Fig. 9, *A* and *B,* and data not shown). This supports the results shown here in Fig. 8 as well as published data (22). Furthermore, we quantified the α1- and α2-associated fluorescent intensity in postsynaptic sites and calculated the $\alpha1/\alpha2$ intensity ratio (ratio $\alpha1/\alpha2$) for $Np^{-/-}$ and $Np^{+/+}$ neurons at 12 (Fig. 9*E, I*) and 21 DIV (Fig. 9*E, II*). This parameter includes gephyrin-positive postsynapses where the $GABA_AR$ α2 subunit is still present, but not those where α2-associated fluorescence is completely absent (see *arrows* in Figs. 8*C*, and 9, *B, I* and *II*). At 12 DIV, $Np^{+/+}$ and $Np^{-/-}$ neurons displayed a similar somatic $\alpha1/\alpha2$ ratio of 0.96 ± 0.04 and 0.94 ± 0.03, respectively (45 neurons, 3 independent cultures, $p = 0.798$, Mann-Whitney *U* test, Fig. 9*E, I*). In dendrites, the $\alpha1/\alpha2$ ratio was 1.07 ± 0.06 and 0.71 ± 0.16 for $Np^{+/+}$ and $Np^{-/-}$ neurons, respectively ($p < 0.05$, Mann-Whitney *U* test, Fig. 9*E, I*). Importantly, the $\alpha1/\alpha2$ ratio was increased in both somata and dendrites of $Np^{-/-}$ compared with $Np^{+/+}$ at 21 DIV. For 21 DIV $Np^{+/+}$ neurons the $\alpha1/\alpha2$ ratios were 1.15 ± 0.5 and 0.95 ± 0.09, whereas for $Np^{-/-}$ neurons the ratios were 1.59 ± 0.31 and 1.36 ± 0.06 in soma and dendrites, respectively ($p < 0.05$, Mann-Whitney *U* test, Fig. 9*E, II*). Thus, Np deficiency increases the relative abundance of α1 as compared with α2 subunits in inhibitory postsynapses.

DISCUSSION

Here we show that Np deficiency leads to a selective structural destabilization of glutamatergic but not GABAergic synapses. Although $Np^{-/-}$ neurons showed an altered localization of $GABA_A$ receptor α2 subunits, we observed no change either in number or matching of post-presynaptic inhibitory compartments. The ratio of glutamatergic *versus* GABAergic synapses was significantly perturbed, and the electrophysiological studies confirmed that transmission at both inhibitory and excitatory synapses is altered as a consequence of Np deficiency. Acute incubation of mature wild-type neurons with recombinant Np65-Fc, but not Np55-Fc mimicked the mutant phenotype at excitatory synapses. Moreover, incubation with an isoform-specific anti-Np65 antibody perturbed excitatory, but not inhibitory presynaptic function as evaluated by synaptotagmin uptake assay. Acute Np65-mediated synaptic stabilization could be assigned predominantly to CA1 and DG, but not CA3 neurons. Although Np65 is present in GABAergic terminals, our data argue for a more restricted and acute role for the *trans* homophilic binding of Np65 in the structural stability of excitatory synapses.

Np65 in Hippocampal Circuits—We show that Np65 is predominantly expressed in CA1 and DG fields of hippocampal slices, which is in good agreement with previous data (20, 23). The number of glutamatergic synaptic contacts was found to be reduced in the CA1 and DG, but not in the CA3 area, of Np-deficient mice. Thus, the reduction in synaptic connections resulting from the mutation occurs in the hippocampal fields where normally Np65 is abundant. Mimicking the *in vivo* situation, dissociated hippocampal neurons with a CA1 or DG signature expressed the highest levels of Np65 compared with other hippocampal neurons, and in cultures obtained from $Np^{-/-}$ mice these neurons displayed the most severe loss of glutamatergic synaptic contacts. Accordingly, the expression of Np65 by CA1 and DG neurons seems to be required for the establishment of both the correct number and function of glutamatergic synapses in specific hippocampal circuits. Similarly another single-pass transmembrane CAM, Cadherin-9, a prototypical class II cadherin, is required specifically for formation of DG to CA3 but not CA1 synapses in culture and in hippocampal slices loss of cadherin-9 disrupts mossy fiber bouton and thorny excrescence spine formation through *trans*-synaptic interactions (8). We therefore propose that, as for Cadherin-9 and others (9), Np65 is one such differentially expressed molecular cue, which contributes to the specific connection of excitatory hippocampal synapses (10).

Np65 Stabilizes Excitatory Synapses—At 12 DIV, we found no change in the number of newly formed excitatory contacts but more mismatched postsynaptic sites, and thus a decreased post- to presynapse matching in $Np^{-/-}$ neurons. After 21 DIV, when synaptic contacts have matured the hallmark finding is that $Np^{-/-}$ neurons display less excitatory synapses, whereas the number of inhibitory contacts is unchanged, resulting in a decreased ratio of excitatory to inhibitory contacts.

Features observed in $Np^{-/-}$ neurons were mimicked by acute application of recombinant Np65-Fc, but not Np55-Fc, to mature wild-type neurons. Thus, we infer that the mutant phenotype reveals a direct acute function of Np65 in stabilization of excitatory synaptic contacts. Np65-Fc, but not Np55-Fc, predominantly attaches to the surface of CA1 and DG neurons

FIGURE 9. **Enlarged postsynaptic sites and altered synaptic α2 to α1 $GABA_A$ receptor subunit ratio of $Np^{-/-}$ neurons.** $Np^{+/+}$ and $Np^{-/-}$ neurons were cultured for 12 (*A*, *C,* and *E, panel I*) and 21 DIV (*B*, *D,* and *E, panel II*), and stained for gephyrin (*gep, gray*), α2 (*cyan*), and α1 (*magenta*) $GABA_AR$ subunits. Somata (*A* and *B*, *panel I*) and dendrites (*A* and *B*, *panel II*) were independently photographed using a confocal microscope and analyzed for the number, size, and fluorescence intensity of gephyrin puncta. *E,* the content of α1 and α2 in gephyrin-positive postsynapses ($\alpha1/\alpha2$ ratio per gephyrin punctum) was calculated using the fluorescence intensities of these $GABA_AR$ subunits co-localizing with gephyrin clusters. Representative pictures and data (mean ± S.E.) are from 3 independent experiments. *Scale bar* in *A* and *B*, *panel I*, = 20 μm, and in *B*, *panel II* = 2 μm. **, $p < 0.01$, or *, $p < 0.05$ between genotypes.

coinciding with the high level of endogenous Np65 in these neuronal types, indicating that endogenous Np65 can act as a receptor of Np65-Fc. This is consistent with Np65, but not Np55, forming homophilic interactions via their Np65-specific Ig1 domain. Furthermore, both extracellular Np65-Fc or anti-Np65-Ig1 domain antibodies impair maintenance of hippocampal CA1 long term potentiation (20) most likely via p38 MAPK-dependent destabilization and internalization of GluA1-containing glutamate receptors from the synaptic membrane (23). Although we observed some attachment of Np65-Fc to the neuronal surface even in $Np^{-/-}$ neurons this is not directly responsible for synaptic destabilization as no further synaptic mismatch was induced by treatment of $Np^{-/-}$ neurons with Np65-Fc. Thus, competition with Np65-Fc could rapidly destabilize pre-existing Np65-containing complexes producing impairment of synaptic function ultimately leading to the loss of functional and structural integrity of excitatory synapses. Consistent with this hypothesis, failed synapse stabilization can be responsible for a lower number of postsynaptic sites (39). Although our experiments argue for an acute function for Np65 at excitatory synapses, they do not fully exclude a potential involvement of extra-synaptic neuroplastin that would further contribute to the mutant phenotype.

Using F-actin we observed a lower number of postsynapses in $Np^{-/-}$ compared with $Np^{+/+}$ neurons (Fig. 2*C*). Moreover F-actin seemed to be abnormally accumulated on the dendritic shaft of the mutant neurons. As actin is the major cytoskeletal component of excitatory spines, and it has been shown that the small RhoA GTPase is a key participant in the mechanism controlling actin polymerization (40), a plausible hypothesis is that Np65 regulates the RhoA activation/deactivation cycle to modulate actin polymerization and thus spine formation/stabilization.

Np65 at Inhibitory Synapses—$GABA_A$Rs containing α2-subunits co-localize with Np65 at the plasma membrane in rat hippocampal neurons. In $Np^{-/-}$ neurons, more α2-immunoreactivity was detected outside VIAAT-positive synapses compared with wild-type indicating that Np65 may be required for the correct localization of α2-containing receptors at inhibitory synapses. Consistent with this result it has been suggested that Np65 may play a role in the localization of $GABA_A$Rs to synapses (22). Here, we show that number and matching of VIAAT to gephyrin-positive synaptic contacts remained normal in $Np^{-/-}$ neurons and Np65-Fc-treated mature $Np^{+/+}$ neurons, indicating that the Np65-$GABA_A$R α2-subunit association may not be crucial for maintenance of inhibitory synapses. In the same direction, a change in $GABA_A$R composition or function is not necessarily accompanied by structural changes of inhibitory synapses (41).

Importantly, we found that inhibitory transmission is impaired in $Np^{-/-}$ neurons in which IPSCs exhibit both increased amplitude and accelerated decay time. These results support a role for Np65 in modulation of $GABA_A$R activity, most probably by coordinating proper α2 subunit-containing $GABA_A$R localization at inhibitory synapses. Indeed, we observed delocalization of the α2 subunit and an increased synaptic α1/α2 ratio in $Np^{-/-}$ neurons. The α2 subunit contributes to the slow decaying of $GABA_A$R-mediated IPSCs as concluded from antisense-mediated α2 subunit down-regulation. This in turn results in up-regulation of α1-containing receptors in synapses and thereby accelerating kinetic decay (42). Indeed, α1 subunits can substitute the α2 subunits in hippocampal neurons from α2-deficient mice (43). Thus, we conclude that Np65 deficiency leads to α2 subunit delocalization thereby switching the composition of $GABA_A$R to a more α1-enriched receptor population. It has been reported that altered $GABA_A$R subunit protein levels, abnormal synaptic location, and modified $GABA_A$R composition impair inhibitory transmission as observed in α1 (44, 45), α2 (43), and α3 null mice (46). These data suggest that interference with the expression of one specific $GABA_A$R α-subunit may produce complex compensatory changes by the others.

Is Np65 a Regulator of the Ratio and Function of Excitatory and Inhibitory Synapses?—Our data suggest that Np deficiency alters the number ratio and the functionality of glutamatergic and GABAergic synapses by distinct and multiple mechanisms. It has been shown that, at 7 DIV when still excitatory synapses are not yet developed, α2-subunit delocalization from GABAergic contacts occurs in anti-Np65 shRNA-transfected rat hippocampal neurons (22). Thus, we conclude that Np deficiency is directly responsible for the phenotype at GABAergic synapses in $Np^{-/-}$ neurons. However, an interaction of the observed GABAergic phenotypes yielding impaired excitatory synapses in $Np^{-/-}$ neurons cannot be excluded. For instance, it is known that early during neuronal network formation GABAergic synapses can be excitatory (48, 49). Therefore, it is possible that the altered composition of $GABA_A$Rs may secondarily affect the development of glutamatergic synapses in $Np^{-/-}$ neurons. The observation that acute interference with Np65 function in excitatory synapses without altering GABAergic synapses adding Np65-Fc or anti-Np65 antibodies (Ref. 20 and 23 and this report) on $Np^{+/+}$ neurons mimics the glutamatergic synaptic phenotype of $Np^{-/-}$ neurons (this report) argues for independent functions of Np65 in glutamatergic and GABAergic synapses.

Our data indicate that Np65 might be involved in the determination of the number of excitatory and inhibitory synapses in the adult brain. In this context, Np65 shows fundamental differences to neuroligins that have been reported as key regulators of the neuronal excitability by regulating E/I balance. First, heterophilic binding of postsynaptic neuroligins to presynaptic neurexins recruits intracellular scaffolds (11, 13, 47). In contrast, postsynaptic Np65 may bind presynaptic Np65 in a homophilic fashion without direct recruitment of synaptic scaffolding proteins as its intracellular domain lacks any known motif able to bind these intracellular proteins. Alternatively, Np65 may structure synapses by organizing synaptic membrane protein complexes, *i.e.* GluA1-containing glutamate receptors (23), $GABA_A$ receptor subunits (22), and others. Second, Np65 acts at a later stage of development and may therefore be implicated in stabilization and maintenance of synapses rather than in their formation as proposed for neuroligins (12, 13). Thus, Np65 function is not redundant but adds a new facet to the proper E/I ratio in neuronal circuits.

Potential Roles for Np65 in the E/I Balance and Brain Function—Disturbed E/I balance in specific brain areas, *i.e.* the hippocampal CA1 region, is a key hypothesis to explain the

development of schizophrenia in patients (50, 51). Interestingly, both Np as well as the $GABA_AR$ subunit $\alpha 2$ have been proposed to play a role in schizophrenia (38, 52). Thus, Np65 is an attractive candidate to mediate the correct balance in specific brain areas whose dysfunction might be relevant for mental pathologies.

In summary, we show that Np65 regulates structural stability and contact of excitatory synapses and the localization of $GABA_AR$ $\alpha 2$ subunits at inhibitory synapses. Our results strongly support a role for Np65 not only in establishing and maintaining of specific hippocampal connections but also in regulating the correct ratio of excitatory to inhibitory synaptic activity. As Np65 is implicated in synaptic plasticity and memory formation (16), it will be interesting to relate Np65-mediated structural stability of synapses and its role in maintaining the correct neuronal network activity in specific brain regions to the complex phenotype displayed by Np-deficient mice.

Acknowledgments—We gratefully acknowledge the assistance of Karla Sowa, Daniela Hill, and Soumee Bhattacharya for providing mice. One of us (R. H-M.) thanks A.-C. Lehmann for critical comments and Dr. Angela Kolodziej for valuable help in staining of mouse sections.

Addendum—After submitting our article for review, we learned of an article to be published by Desrivières *et al.* (53). This new study provides evidence for a critical role of neuroplastin in individual intellectual differences and further supports the association of neuroplastin with schizophrenia. Furthermore, in human neuroplastin, as a target of FOXP2 (54), may be linked to speech development. Altogether the new data further support important functions of neuroplastin in the human brain. Our data, describing at the synaptic level the functional role of neuroplastin, are thus in our view of high interest to a broad readership.

REFERENCES

1. Benson, D. L., and Huntley, G. W. (2012) Synapse adhesion: a dynamic equilibrium conferring stability and flexibility. *Curr. Opin. Neurobiol.* **22,** 397–404
2. Lüthl, A., Laurent, J. P., Figurov, A., Muller, D., and Schachner, M. (1994) Hippocampal long-term potentiation and neural cell adhesion molecules L1 and NCAM. *Nature* **372,** 777–779
3. Rønn, L. C., Bock, E., Linnemann, D., and Jahnsen, H. (1995) NCAM-antibodies modulate induction of long-term potentiation in rat hippocampal CA1. *Brain Research* **677,** 145–151
4. Tang, L., Hung, C. P., and Schuman, E. M. (1998) A role for the cadherin family of cell adhesion molecules in hippocampal long-term potentiation. *Neuron* **20,** 1165–1175
5. Sakurai, E., Hashikawa, T., Yoshihara, Y., Kaneko, S., Satoh, M., and Mori, K. (1998) Involvement of dendritic adhesion molecule telencephalin in hippocampal long-term potentiation. *Neuroreport* **9,** 881–886
6. Lauri, S. E., Kaukinen, S., Kinnunen, T., Ylinen, A., Imai, S., Kaila, K., Taira, T., and Rauvala, H. (1999) Regulatory role and molecular interactions of a cell-surface heparan sulfate proteoglycan (N-syndecan) in hippocampal long-term potentiation. *J. Neurosci.* **19,** 1226–1235
7. Contractor, A., Rogers, C., Maron, C., Henkemeyer, M., Swanson, G. T., and Heinemann, S. F. (2002) Trans-synaptic Eph receptor-ephrin signaling in hippocampal mossy fiber LTP. *Science* **296,** 1864–1869
8. Williams, M. E., Wilke, S. A., Daggett, A., Davis, E., Otto, S., Ravi, D., Ripley, B., Bushong, E. A., Ellisman, M. H., Klein, G., and Ghosh, A. (2011) Cadherin-9 regulates synapse-specific differentiation in the developing hippocampus. *Neuron* **71,** 640–655
9. Sylwestrak, E. L., and Ghosh, A. (2012) Elfn1 regulates target-specific release probability at CA1-interneuron synapses. *Science* **338,** 536–540
10. Williams, M. E., de Wit, J., and Ghosh, A. (2010) Molecular mechanisms of synaptic specificity in developing neural circuits. *Neuron* **68,** 9–18
11. Chubykin, A. A., Atasoy, D., Etherton, M. R., Brose, N., Kavalali, E. T., Gibson, J. R., and Südhof, T. C. (2007) Activity-dependent validation of excitatory versus inhibitory synapses by neuroligin-1 versus neuroligin-2. *Neuron* **54,** 919–931
12. Südhof, T. C. (2008) Neuroligins and neurexins link synaptic function to cognitive disease. *Nature* **455,** 903–911
13. Chih, B., Engelman, H., and Scheiffele, P. (2005) Control of excitatory and inhibitory synapse formation by neuroligins. *Science* **307,** 1324–1328
14. Deleted in proof
15. Langnaese, K., Beesley, P. W., and Gundelfinger, E. D. (1997) Synaptic membrane glycoproteins gp65 and gp55 are new members of the immunoglobulin superfamily. *J. Biol. Chem.* **272,** 821–827
16. Owczarek, S., and Berezin, V. (2012) Neuroplastin: cell adhesion molecule and signaling receptor. *Int. J. Biochem. Cell Biol.* **44,** 1–5
17. Kreutz, M. R., Langnaese, K., Dieterich, D. C., Seidenbecher, C. I., Zuschratter, W., Beesley, P. W., and Gundelfinger, E. D. (2001) Distribution of transcript and protein isoforms of the synaptic glycoprotein neuroplastin in rat retina. *Invest. Ophthalmol. Vis. Sci.* **42,** 1907–1914
18. Boyken, J., Grønborg, M., Riedel, D., Urlaub, H., Jahn, R., and Chua, J. J. (2013) Molecular profiling of synaptic vesicle docking sites reveals novel proteins but few differences between glutamatergic and GABAergic synapses. *Neuron* **78,** 285–297
19. Watson, R. E., Desesso, J. M., Hurtt, M. E., and Cappon, G. D. (2006) Postnatal growth and morphological development of the brain: a species comparison. *Birth Defects Res. B. Dev. Reprod. Toxicol.* **77,** 471–484
20. Smalla, K. H., Matthies, H., Langnäse, K., Shabir, S., Böeckers, T. M., Wyneken, U., Staak, S., Krug, M., Beesley, P. W., and Gundelfinger, E. D. (2000) The synaptic glycoprotein neuroplastin is involved in long-term potentiation at hippocampal CA1 synapses. *Proc. Natl. Acad. Sci. U.S.A.* **97,** 4327–4332
21. Owczarek, S., Soroka, V., Kiryushko, D., Larsen, M. H., Yuan, Q., Sandi, C., Berezin, V., and Bock, E. (2011) Neuroplastin-65 and a mimetic peptide derived from its homophilic binding site modulate neuritogenesis and neuronal plasticity. *J. Neurochem.* **117,** 984–994
22. Sarto-Jackson, I., Milenkovic, I., Smalla, K. H., Gundelfinger, E. D., Kaehne, T., Herrera-Molina, R., Thomas, S., Kiebler, M. A., and Sieghart, W. (2012) The cell adhesion molecule neuroplastin-65 is a novel interaction partner of γ-aminobutyric acid type A receptors. *J. Biol. Chem.* **287,** 14201–14214
23. Empson, R. M., Buckby, L. E., Kraus, M., Bates, K. J., Crompton, M. R., Gundelfinger, E. D., and Beesley, P. W. (2006) The cell adhesion molecule neuroplastin-65 inhibits hippocampal long-term potentiation via a mitogen-activated protein kinase p38-dependent reduction in surface expression of GluR1-containing glutamate receptors. *J. Neurochem.* **99,** 850–860
24. Lazarevic, V., Schöne, C., Heine, M., Gundelfinger, E. D., and Fejtova, A. (2011) Extensive remodeling of the presynaptic cytomatrix upon homeostatic adaptation to network activity silencing. *J. Neurosci.* **31,** 10189–10200
25. Nagy, A., Moens, C., Ivanyi, E., Pawling, J., Gertsenstein, M., Hadjantonakis, A. K., Pirity, M., and Rossant, J. (1998) Dissecting the role of N-myc in development using a single targeting vector to generate a series of alleles. *Curr. Biol.* **8,** 661–664
26. Montag, D., Giese, K. P., Bartsch, U., Martini, R., Lang, Y., Blüthmann, H., Karthigasan, J., Kirschner, D. A., Wintergerst, E. S., Nave, K.-A., Zielasek, J., Toyka, K. V., Lipp, H.-P., and Schachner, M. (1994) Mice deficient for the myelin-associated glycoprotein show subtle abnormalities in myelin. *Neuron* **13,** 229–246
27. Herrera-Molina, R., Flores, B., Orellana, J. A., and von Bernhardi, R. (2012) Modulation of interferon-γ-induced glial cell activation by transforming growth factor β1: a role for STAT1 and MAPK pathways. *J. Neurochem.* **123,** 113–123
28. Herrera-Molina, R., Frischknecht, R., Maldonado, H., Seidenbecher, C. I., Gundelfinger, E. D., Hetz, C., Aylwin Mde, L., Schneider, P., Quest, A. F.,

and Leyton, L. (2012) Astrocytic αVβ3 integrin inhibits neurite outgrowth and promotes retraction of neuronal processes by clustering Thy-1. *PloS One* **7,** e34295
29. Ippolito, D. M., and Eroglu, C. (2010) Quantifying synapses: an immunocytochemistry-based assay to quantify synapse number. *J. Vis. Exp.* **45,** 2270
30. Megías, M., Emri, Z., Freund, T. F., and Gulyás, A. I. (2001) Total number and distribution of inhibitory and excitatory synapses on hippocampal CA1 pyramidal cells. *Neuroscience* **102,** 527–540
31. Wouterlood, F. G., Boekel, A. J., Kajiwara, R., and Beliën, J. A. (2008) Counting contacts between neurons in 3D in confocal laser scanning images. *J. Neurosci. Methods* **171,** 296–308
32. Tsuriel, S., Geva, R., Zamorano, P., Dresbach, T., Boeckers, T., Gundelfinger, E. D., Garner, C. C., and Ziv, N. E. (2006) Local sharing as a predominant determinant of synaptic matrix molecular dynamics. *PLoS Biol.* **4,** e271
33. Hering, H., and Sheng, M. (2001) Dendritic spines: structure, dynamics and regulation. *Nat. Rev. Neurosci.* **2,** 880–888
34. Rao, A., Cha, E. M., and Craig, A. M. (2000) Mismatched appositions of presynaptic and postsynaptic components in isolated hippocampal neurons. *J. Neurosci.* **20,** 8344–8353
35. Anderson, T. R., Shah, P. A., and Benson, D. L. (2004) Maturation of glutamatergic and GABAergic synapse composition in hippocampal neurons. *Neuropharmacology* **47,** 694–705
36. Arlotta, P., Molyneaux, B. J., Chen, J., Inoue, J., Kominami, R., and Macklis, J. D. (2005) Neuronal subtype-specific genes that control corticospinal motor neuron development *in vivo*. *Neuron* **45,** 207–221
37. Bagri, A., Gurney, T., He, X., Zou, Y. R., Littman, D. R., Tessier-Lavigne, M., and Pleasure, S. J. (2002) The chemokine SDF1 regulates migration of dentate granule cells. *Development* **129,** 4249–4260
38. Engin, E., Liu, J., and Rudolph, U. (2012) α2-containing $GABA_A$ receptors: a target for the development of novel treatment strategies for CNS disorders. *Pharmacol. Ther.* **136,** 142–152
39. Mendez, P., De Roo, M., Poglia, L., Klauser, P., and Muller, D. (2010) N-cadherin mediates plasticity-induced long-term spine stabilization. *J. Cell Biol.* **189,** 589–600
40. Schubert, V., Da Silva, J. S., and Dotti, C. G. (2006) Localized recruitment and activation of RhoA underlies dendritic spine morphology in a glutamate receptor-dependent manner. *J. Cell Biol.* **172,** 453–467
41. Zhang, C., Atasoy, D., Araç, D., Yang, X., Fucillo, M. V., Robison, A. J., Ko, J., Brunger, A. T., and Südhof, T. C. (2010) Neurexins physically and functionally interact with GABA(A) receptors. *Neuron* **66,** 403–416
42. Brussaard, A. B., Kits, K. S., Baker, R. E., Willems, W. P., Leyting-Vermeulen, J. W., Voorn, P., Smit, A. B., Bicknell, R. J., and Herbison, A. E. (1997) Plasticity in fast synaptic inhibition of adult oxytocin neurons caused by switch in $GABA_A$ receptor subunit expression. *Neuron* **19,** 1103–1114
43. Panzanelli, P., Gunn, B. G., Schlatter, M. C., Benke, D., Tyagarajan, S. K., Scheiffele, P., Belelli, D., Lambert, J. J., Rudolph, U., and Fritschy, J. M. (2011) Distinct mechanisms regulate $GABA_A$ receptor and gephyrin clustering at perisomatic and axo-axonic synapses on CA1 pyramidal cells. *J. Physiol.* **589,** 4959–4980
44. Ortinski, P. I., Lu, C., Takagaki, K., Fu, Z., and Vicini, S. (2004) Expression of distinct α subunits of $GABA_A$ receptor regulates inhibitory synaptic strength. *J. Neurophysiol.* **92,** 1718–1727
45. Schneider Gasser, E. M., Duveau, V., Prenosil, G. A., and Fritschy, J. M. (2007) Reorganization of GABAergic circuits maintains $GABA_A$ receptor-mediated transmission onto CA1 interneurons in alpha1-subunit-null mice. *Eur. J. Neurosci.* **25,** 3287–3304
46. Winsky-Sommerer, R., Knapman, A., Fedele, D. E., Schofield, C. M., Vyazovskiy, V. V., Rudolph, U., Huguenard, J. R., Fritschy, J. M., and Tobler, I. (2008) Normal sleep homeostasis and lack of epilepsy phenotype in $GABA_A$ receptor α3 subunit-knockout mice. *Neuroscience* **154,** 595–605
47. Giannone, G., Mondin, M., Grillo-Bosch, D., Tessier, B., Saint-Michel, E., Czöndör, K., Sainlos, M., Choquet, D., and Thoumine, O. (2013) Neurexin-1β binding to neuroligin-1 triggers the preferential recruitment of PSD-95 versus gephyrin through tyrosine phosphorylation of neuroligin-1. *Cell Reports* **3,** 1996–2007
48. Ben-Ari, Y., Tseeb, V., Raggozzino, D., Khazipov, R., and Gaiarsa, J. L. (1994) γ-Aminobutyric acid (GABA): a fast excitatory transmitter which may regulate the development of hippocampal neurones in early postnatal life. *Prog. Brain Res.* **102,** 261–273
49. Cherubini, E., Gaiarsa, J. L., and Ben-Ari, Y. (1991) GABA: an excitatory transmitter in early postnatal life. *Trends Neurosci.* **14,** 515–519
50. Lisman, J. (2012) Excitation, inhibition, local oscillations, or large-scale loops: what causes the symptoms of schizophrenia? *Curr. Opin. Neurobiol.* **22,** 537–544
51. Schobel, S. A., Lewandowski, N. M., Corcoran, C. M., Moore, H., Brown, T., Malaspina, D., and Small, S. A. (2009) Differential targeting of the CA1 subfield of the hippocampal formation by schizophrenia and related psychotic disorders. *Arch. Gen. Psychiatry* **66,** 938–946
52. Saito, A., Fujikura-Ouchi, Y., Kuramasu, A., Shimoda, K., Akiyama, K., Matsuoka, H., and Ito, C. (2007) Association study of putative promoter polymorphisms in the neuroplastin gene and schizophrenia. *Neurosci. Lett.* **411,** 168–173
53. Desrivières, S., Lourdusamy, A., Tao, C., Toro, R., Jia, T., Loth, E., Medina, L. M., Kepa, A., Fernandes, A., Ruggeri, B., Carvalho, F. M., Cocks, G., Banaschewski, T., Barker, G. J., Bokde, A. L. W., Büchel, C., Conrod, P. J., Flor, H., Heinz, A., Gallinat, J., Garavan, H., Gowland, P., Brühl, R., Lawrence, C., Mann, K., Martinot, M. L. P., Nees, F., Lathrop, M., Poline, J.-B., Rietschel, M., Thompson, P., Fauth-Bühler, M., Smolka, M. N., Pausova, Z., Paus, T., Feng, J., Schumann, G., and the IMAGEN Consortium (2014) Single nucleotide polymorphism in the neuroplastin locus associates with cortical thickness and intellectual ability in adolescents. *Mol. Psychiatry* 10.1038/mp.2013.197
54. Vernes, S. C., Oliver, P. L., Spiteri, E., Lockstone, H. E., Puliyadi, R., Taylor, J. M., Ho, J., Mombereau, C., Brewer, A., Lowy, E., Nicod, J., Groszer, M., Baban, D., Sahgal, N., Cazier, J. B., Ragoussis, J., Davies, K. E., Geschwind, D. H., and Fisher, S. E. (2011) Foxp2 regulates gene networks implicated in neurite outgrowth in the developing brain. *PLoS Genet.* **7,** e1002145